Journal of Medicinal Chemistry

Article

Functional Selectivity Revealed by *N*-Methylation Scanning of Human Urotensin II and Related Peptides

Francesco Merlino, Etienne Billard, Ali Munaim Yousif, Salvatore Di Maro, Diego Brancaccio, Luigi Abate, Alfonso Carotenuto, Rosa Bellavita, Roberta d'Emmanuele di Villa Bianca, Paolo Santicioli, Luciana Marinelli, Ettore Novellino, Terence Hébert, William D. Lubell, David Chatenet, and Paolo Grieco

J. Med. Chem., **Just Accepted Manuscript** • DOI: 10.1021/acs.jmedchem.8b01601 • Publication Date (Web): 07 Jan 2019

Functional Selectivity Revealed by *N*-Methylation Scanning of Human Urotensin II and Related Peptides

Francesco Merlino,[†,‡] Étienne Billard,[∫,‡] Ali M. Yousif,[†] Salvatore Di Maro,[†,Ω] Diego Brancaccio,[†] Luigi Abate,[†] Alfonso Carotenuto,[†] Rosa Bellavita,[†] Roberta d'Emmanuele di Villa Bianca,[†] Paolo Santicioli,[§] Luciana Marinelli,[†] Ettore Novellino,[†] Terence E. Hébert,[#] William D. Lubell,[∏] David Chatenet,[,∫] and Paolo Grieco*[,†]*

[†]Department of Pharmacy, University of Naples 'Federico II', via D. Montesano 49, 80131 Naples, Italy; [∫]INRS - Institut Armand-Frappier, Groupe de Recherche en Ingénierie des Peptides et en Pharmacothérapie (GRIPP), Université du Québec, 531 Boulevard des Prairies, Ville de Laval, Québec H7V 1B7, Canada; [§]Department of Pharmacology, Menarini Ricerche, via Rismondo 12/A, 50131 Florence, Italy; [∏]Département de Chimie, Université de Montréal, C.P. 6128, Station Centre-ville, Montréal, Québec H3C 3J7, Canada; [#]Department of Pharmacology and Therapeutics, McGill University, Montréal, Québec H3A 1A3, Canada.

ABSTRACT

In accordance with their common but also divergent physiological actions, human urotensin II (*h*U-II, **1**) and urotensin II-related peptide (URP, **2**) could stabilize specific urotensin II receptor

(UTR) conformations, thereby activating different signalling pathways, a feature referred to as biased agonism or functional selectivity. Sequential *N*-methylation of the amides in the conserved core sequence of **1**, **2** and fragment U-II$_{4-11}$ (**3**) shed light on structural requirements involved in their functional selectivity. Thus, eighteen *N*-methylated UTR ligands were synthesized and their biological profiles evaluated using both *in vitro* competition binding assays, *ex vivo* rat aortic ring bioassays and BRET-based biosensor experiments. Biological activity diverged from that of the parent structures contingent on the location of amide methylation indicating relevant hydrogen-bond interactions for function of the endogenous peptides. Conformational analysis of selected *N*-methyl analogs indicated the importance of specific amide residues of **2** for the distinct pharmacology relative to **1** and **3**.

INTRODUCTION

Among the available synthetic strategies to modify peptide structures,[1-3] *N*-methylation of amide bonds has become an attractive tool.[4-6] *N*-Methylation creates tertiary amide bonds that may exhibit *cis*-*trans* isomer equilibrium due to increased steric hindrance with adjacent amino acid side chains.[7,8] Moreover, replacement of the amide hydrogen by a methyl group may disrupt intra- and inter-molecular hydrogen-bonds, which may be respectively important for stabilization of bioactive conformations and for receptor recognition.[9] Introduction of *N*-methyl amides may thus have significant consequences on both pharmacodynamics and pharmacokinetic properties.[6,10]

Considering peptides as relatively flexible and metabolically unstable,[11] susceptibility to proteolytic degradation, poor absorption and short *in vivo* half-life,[2,3] all may be considered their unfavorable pharmacokinetic properties that hinder therapeutic applications.[12,13] In this regard,

N-methylation of amide bonds in peptides may overcome such limitations by improving both stability and bioavailability, correlated with increased activity and selectivity.[4,9,14,15] *N*-Methylation of multiple peptide bonds may have complementary effects to improve bioavailability and target (*e.g.*, receptor subtype) selectivity.[15-17] Driven in part by the success of natural *N*-methylated peptides, such as the immunosuppressant drug cyclosporine A and the nematicide omphalotin,[18,19] *N*-methylation has been pursued to improve "drug-like" properties,[10] in a wide range of peptides possessing antibiotic,[20] anticancer,[21] as well as various other activities.[22] To our knowledge however, backbone *N*-methylation has never been investigated as a tool to reveal functional selectivity that represents the ligand-dependent selectivity for certain signal transduction pathways relative to the native ligand of the receptor.[23]

The urotensinergic system,[24] consisting of two endogenous ligands, *i.e.* urotensin II and urotensin II-related peptide [*h*U-II (**1**) and URP (**2**), Chart 1], and their G protein-coupled receptor (GPCR) termed UTR, is involved in several patho-physiological conditions in humans.[25,26] Accordingly, several UTR antagonists, such as 1-[2-(4-benzyl-4-hydroxy-piperidin-1-yl)-ethyl]-3-(2-methyl-quinolin-4-yl)-urea sulfate salt (ACT-058362, also known as Palosuran),[27] 4′-[(1*R*)-1-[[(6,7-dichloro-3-oxo-2,3-dihydro-4H-1,4-benzoxazin-4-yl)-acetyl](methyl)amino]-2-(4-morpholinyl)ethyl]-4-biphenylcarboxylicacid trifluoroacetate (GSK1440115),[28] and 2-bromo-*N*-[4-chloro-3-((*R*)-1-methyl-pyrrolidin-3-yloxy)-phenyl]-4,5-dimethoxybenzenesulphonamide hydrochloride (SB-657510),[29] have been shown to protect against renal ischemia,[27] asthma,[28] liver fibrosis,[30] and pulmonary hypertension in rodents.[31] However, none of these candidates exhibited efficacy in clinical trials.[25]

Although studies *in vitro* using HEK 293 cells have failed to show differences in the signaling signatures of endogenous UTR ligands, in target tissues, distinct actions of **1** and **2**

have been demonstrated on transcription initiation, astrocyte proliferation, polyphosphoinositide turnover, ANP release, and myocardial contraction.[24,25] Structure-activity relationship (SAR) studies have demonstrated that the intra-cyclic residues of isoforms of **1** and **2** play critical roles in both recognition and activation of UTR.[25,26] Likewise, SAR studies of both peptides were usually similar, but, in certain cases, striking differences were noted despite the introduction of identical modifications.[26] The *N*-terminal region of **1** differs across species. On binding, the *N*-terminal tail of **1** has been suggested to cause the UTR to undergo a conformational change to accommodate the Trp-Lys-Tyr triad of the cyclic peptide.[32-34] Therefore, differences in the signaling signatures of **1** and **2** may be due in part to structural variance at their *N*-terminal regions leading to alternate receptor binding modes. Accordingly, salt bridges between Glu^{1} and Lys^{196} and between Asp^{4} and Arg^{193} have been observed in the **1**-UTR complex, as supported by conformational and docking studies.[35] Considering that understanding of ligand-receptor interactions and their consequences on UTR molecular pharmacology is necessary to reveal divergent signaling pathways (functional selectivity),[23,36] probes to dissect the distinct UTR signaling outcomes in responses to **1** or **2** are essential for assigning specific roles in cell homeostasis and pathogenesis in UTR-associated diseases.[25,37]

Systematic *N*-methyl scanning of the cyclic peptide sequences of UTR ligands **1**-**3** may offer a way to examine the molecular determinants of functional selectivity. The syntheses of *N*-methylated derivatives of **1**, its paralogue peptide **2** and truncated, equally active analog $U\text{-}II_{4\text{-}11}$ (**3**), all were pursued for subsequent biological evaluations using a combination of radioligand binding experiments, *ex vivo* aortic ring contraction assays, and *in vitro* evaluation of G_q activation. Finally, conformational analyses were performed on selected analogs. Notably, *N*-

methylation of the amides of three residues Phe[3/6], Trp[4/7] and Cys[7/10] were identified to affect the biological properties of analogs of **2** in ways that diverged from those exhibited by **1** and **3**.

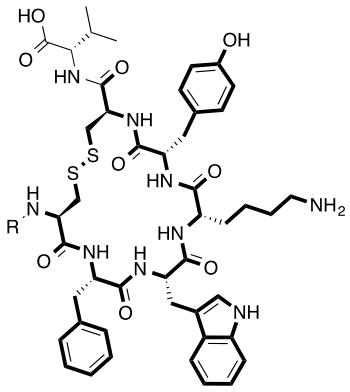

Chart 1. Chemical structures of *h*U-II (**1**), URP (**2**) and U-II$_{4\text{-}11}$ (**3**).

RESULTS AND DISCUSSION

Design. Mono *N*-methylation has been used for years to alter the pharmacological properties of peptides.[4,14] Considering that the *N*-terminal segments of **1** and **2** likely act as molecular discriminators for binding and activation processes by way of stabilization of different receptor conformational subpopulations, these residues were not methylated. Instead, amides of residues within the common cyclic region present in **1**-**3** were replaced systematically by their corresponding N^{α}-methyl counterpart to provide derivatives **4-21** for head-to-head comparisons (Table 1).

Table 1. Peptides **1-3** with *N*-methylation sites as red-highlighted and *N*-(methyl)peptide sequences **4-21**.

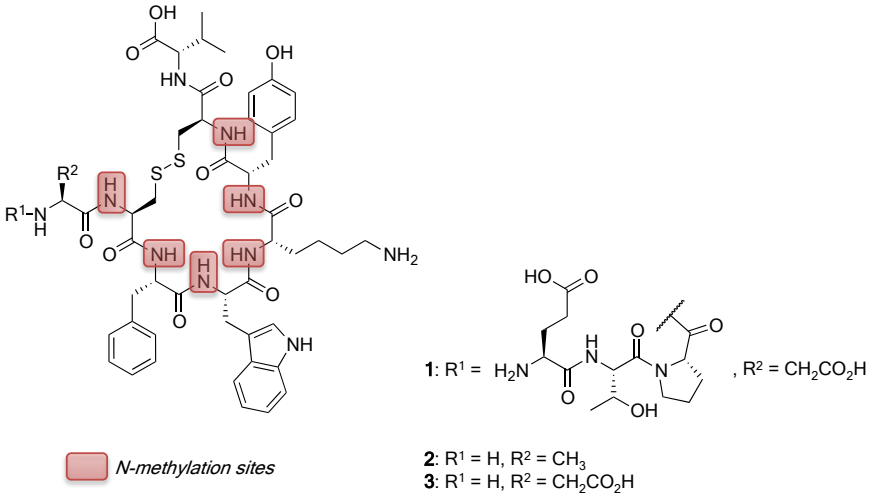

Cmpd	Sequence
[(*N*-Me)Cys^{5}]*h*U-II (**4**)	Glu-Thr-Pro-Asp-*c*[**(*N*-Me)Cys**-Phe-Trp-Lys-Tyr-Cys]-Val
[(*N*-Me)Phe^{6}]*h*U-II (**5**)	Glu-Thr-Pro-Asp-*c*[Cys-**(*N*-Me)Phe**-Trp-Lys-Tyr-Cys]-Val
[(*N*-Me)Trp^{7}]*h*U-II (**6**)	Glu-Thr-Pro-Asp-*c*[Cys-Phe-**(*N*-Me)Trp**-Lys-Tyr-Cys]-Val
[(*N*-Me)Lys^{8}]*h*U-II (**7**)	Glu-Thr-Pro-Asp-*c*[Cys-Phe-Trp-**(*N*-Me)Lys**-Tyr-Cys]-Val
[(*N*-Me)Tyr^{9}]*h*U-II (**8**)	Glu-Thr-Pro-Asp-*c*[Cys-Phe-Trp-Lys-**(*N*-Me)Tyr**-Cys]-Val
[(*N*-Me)Cys^{10}]*h*U-II (**9**)	Glu-Thr-Pro-Asp-*c*[Cys-Phe-Trp-Lys-Tyr-**(*N*-Me)Cys**]-Val
[(*N*-Me)Cys^{2}]URP (**10**)	Ala-*c*[**(*N*-Me)Cys**-Phe-Trp-Lys-Tyr-Cys]-Val
[(*N*-Me)Phe^{3}]URP (**11**)	Ala-*c*[Cys-**(*N*-Me)Phe**-Trp-Lys-Tyr-Cys]-Val
[(*N*-Me)Trp^{4}]URP (**12**)	Ala-*c*[Cys-Phe-**(*N*-Me)Trp**-Lys-Tyr-Cys]-Val
[(*N*-Me)Lys^{5}]URP (**13**)	Ala-*c*[Cys-Phe-Trp-**(*N*-Me)Lys**-Tyr-Cys]-Val
[(*N*-Me)Tyr^{6}]URP (**14**)	Ala-*c*[Cys-Phe-Trp-Lys-**(*N*-Me)Tyr**-Cys]-Val
[(*N*-Me)Cys^{7}]URP (**15**)	Ala-*c*[Cys-Phe-Trp-Lys-Tyr-**(*N*-Me)Cys**]-Val

[(*N*-Me)Cys^5]U-II$_{4-11}$ (**16**)	Asp-*c*[**(*N*-Me)Cys**-Phe-Trp-Lys-Tyr-Cys]-Val
[(*N*-Me)Phe^6]U-II$_{4-11}$ (**17**)	Asp-*c*[Cys-**(*N*-Me)Phe**-Trp-Lys-Tyr-Cys]-Val
[(*N*-Me)Trp^7]U-II$_{4-11}$ (**18**)	Asp-*c*[Cys-Phe-**(*N*-Me)Trp**-Lys-Tyr-Cys]-Val
[(*N*-Me)Lys^8]U-II$_{4-11}$ (**19**)	Asp-*c*[Cys-Phe-Trp-**(*N*-Me)Lys**-Tyr-Cys]-Val
[(*N*-Me)Tyr^9]U-II$_{4-11}$ (**20**)	Asp-*c*[Cys-Phe-Trp-Lys-**(*N*-Me)Tyr**-Cys]-Val
[(*N*-Me)Cys^{10}]U-II$_{4-11}$ (**21**)	Asp-*c*[Cys-Phe-Trp-Lys-Tyr-**(*N*-Me)Cys**]-Val

Chemistry. Peptides **4-21** were produced by solid-phase peptide synthesis (SPPS) using 9-fluorenylmethoxycarbonyl (Fmoc)-chemistry, as previously reported.[38,39] To insert *N*-methyl amide bonds into peptides, commercially available N^{α}-Fmoc-N^{α}-methyl-α-amino acids can be employed, although they are relatively expensive. *N*-Methyl amino acid building blocks have also been synthesized in solution[40] and by solid-phase methods.[41] A solid-phase *N*-methylation procedure was pursued to favor library synthesis of *N*-methyl-peptides (Scheme S1, see Supporting Information). The solid-phase protocol was based on reported methods that proved compatible with most amino acids.[4,41,42] Although methylation using DBU as base and dimethyl sulfate as alkylating agent in NMP was typically completed in 5 min,[4] loss of the trityl protection of the cysteine side chains diminished product quality,[40,41] such that a Mitsunobu reaction procedure was developed to prepare derivatives **4-21**.[43,44] Coupling to *N*-methyl amino acids has been found to be challenging due to steric hindrance. Employment of HATU and HOAt as coupling reagents in combination with DIEA as base in NMP favored acylation of the *N*-methyl peptide.[45] Overall, the *N*-methylation method was effective for synthesizing a library of mono-*N*-methyl derivatives of **1-3** (analogs **4-21**, Table 1). After cleavage peptides were purified by reverse-phase (RP) high-pressure liquid chromatography (HPLC). Each peptide (**4-21**) was

ascertained to be of >98% purity by analytical RP-HPLC in two solvent systems, and exhibited the expected molecular ion on analysis by high-resolution mass (HRMS) spectrometry (LTQ Orbitrap) (Table S1 and Figures S1-10 for the most representative analogues, see Supporting Information).

Biological evaluations. The propensity of each analog to bind UTR was initially evaluated using a competition binding assay. *N*-Methylated analogs **4-21** were examined on either HEK 293 or CHO-K1 cells stably expressing the human UTR isoform. The peptides exhibited varying degrees of binding affinity for the human UTR (Table 2). *N*-Methylation of the amides at the Phe$^{6/3}$, Lys$^{8/5}$ and Tyr$^{9/6}$ residues of peptides **1-3** resulted in a dramatic loss of binding affinity, but had no major effect at the Trp$^{7/4}$ residue. The Phe^{6}-Trp^{7}-Lys^{8}-Tyr^{9} segment in the ring of **1** has previously been suggested to adopt a turn conformation that is stabilized by hydrogen bonds between Phe^{6} NH and Tyr^{9} CO and between Phe^{6} CO and Tyr^{9} NH.[46] The loss of affinity exhibited by **5**, **8**, **11**, **14**, **17** and **20** highlighted further the importance of such a hydrogen-bond network for binding affinity of the parent peptides **1-3**, while *N*-Methylation of the amides of cysteine residues had a slight effect on binding affinity.

In general, *N*-methylation diminished binding affinity relative to the parent peptides **1-3**. The decrease in binding affinity on *N*-methylation was exhibited more profoundly by analogs of **1** (*e.g.*, **4-9**) compared to its smaller counterparts **2** (*e.g.*, **10-15**) and **3** (*e.g.*, **16-21**) (Table 2). The *N*-terminal domain of **1** has recently been demonstrated to be involved in specific receptor interactions that may modulate the receptor binding pocket.[35,47] Hence, the decreased tolerance of *N*-methylation on longer relative to shorter peptides may reflect a diminution of the ability of the receptor to accommodate the bulkier peptide tail.

N-Methyl peptides **4-21** were next tested for ability to induce aortic ring contraction. Similar potency and efficacy compared to **1** was exhibited in an aortic ring contraction assay by analogs possessing *N*-methylation at Cys^5 (*e.g.*, **4**), Trp^7 (*e.g.*, **6**) and Cys^{10} (*e.g.*, **9**); however, *N*-methyl amides at Phe^6, Lys^8 and Tyr^9 (analogs **5**, **7** and **8**) decreased significantly contractile potency (Table 2, Figure 1a), producing weak agonists. Reduced contractile potency of **5** and **8** correlated with their weaker binding affinity and may likely be due to disruption of essential hydrogen bonds for the active secondary structure. The deleterious effect of *N*-methylation at Lys^8 (*e.g.*, **7**) has not been previously reported and may reflect engagement of the amide NH in a hydrogen bond. Although [(*N*-Me)Cys^5]*h*U-II (**4**) and [(*N*-Me)Trp^7]*h*U-II (**6**) exhibited lower affinity than **1**, they retained similar contractile potency as the parent peptide.

Table 2. Binding affinity and contractile activity of **1**, **2** and **3** and related *N*-methyl analogs **4-21**.

Peptide	*Binding affinity*	*Aortic ring contraction*	
	pK_i[a]	pEC_{50}[b]	E_{max}[c]
*h*U-II (**1**)	8.11 ± 0.07	8.52 ± 0.11	102 ± 4
URP (**2**)	8.20 ± 0.12	8.11 ± 0.06	116 ± 4
U-II_{4-11} (**3**)	8.34 ± 0.04	8.28 ± 0.12	100 ± 4
[(*N*-Me)Cys^5]*h*U-II (**4**)	7.31 ± 0.14**	8.01 ± 0.14	112 ± 4
[(*N*-Me)Phe^6]*h*U-II (**5**)	6.09 ± 0.20***	6.70 ± 0.30***	96 ± 10
[(*N*-Me)Trp^7]*h*U-II (**6**)	7.69 ± 0.09*	8.24 ± 0.42	97 ± 10
[(*N*-Me)Lys^8]*h*U-II (**7**)	5.68 ± 0.31***	72% @ 10 μM	
[(*N*-Me)Tyr^9]*h*U-II (**8**)	5.67 ± 0.48***	71% @ 10 μM	
[(*N*-Me)Cys^{10}]*h*U-II (**9**)	7.64 ± 0.15*	7.61 ± 0.10**	105 ± 3
[(*N*-Me)Cys^2]URP (**10**)	8.76 ± 0.07*	8.31 ± 0.19	110 ± 6
[(*N*-Me)Phe^3]URP (**11**)	6.61 ± 0.06***	51% @ 10 μM	
[(*N*-Me)Trp^4]URP (**12**)	8.66 ± 0.13*	7.08 ± 0.45***	35 ± 5***
[(*N*-Me)Lys^5]URP (**13**)	5.82 ± 0.21***	22% @ 10 μM	
[(*N*-Me)Tyr^6]URP (**14**)	5.27 ± 0.84***	16% @ 10 μM	
[(*N*-Me)Cys^7]URP (**15**)	8.45 ± 0.15	8.02 ± 0.49	44 ± 6***
[(*N*-Me)Cys^5]U-II_{4-11} (**16**)	8.53 ± 0.08	8.35 ± 0.15	101 ± 8
[(*N*-Me)Phe^6]U-II_{4-11} (**17**)	6.64 ± 0.10***	6.27 ± 0.09***	98 ± 5
[(*N*-Me)Trp^7]U-II_{4-11} (**18**)	8.76 ± 0.07**	8.47 ± 0.09	105 ± 5
[(*N*-Me)Lys^8]U-II_{4-11} (**19**)	< 5	42% @10 μM	

[(*N*-Me)Tyr^{9}]U-II$_{4-11}$ (**20**)	< 5	44% @10 μM	
[(*N*-Me)Cys^{10}]U-II$_{4-11}$ (**21**)	8.45 ± 0.05	8.28 ± 0.11	95 ± 5

[a]pK$_i$: −logK$_i$; [b]pEC$_{50}$: −log EC$_{50}$; [c]maximum efficacy is expressed as a percentage of the KCl-induced contraction (40 mM) divided by the tissue-response induced by **1** (10^{-7} M). All values are expressed as mean ± S.E.M. Statistical analysis were performed using unpaired Student's t test, $*P \leq 0.05$, $**P \leq 0.01$, $***P \leq 0.001$, *versus* values obtained for **1** (**4-9**), **2** (**10-15**), or **3** (**16-21**). Each replicate (n) was conducted on tissue from different animals or on different cell passages.

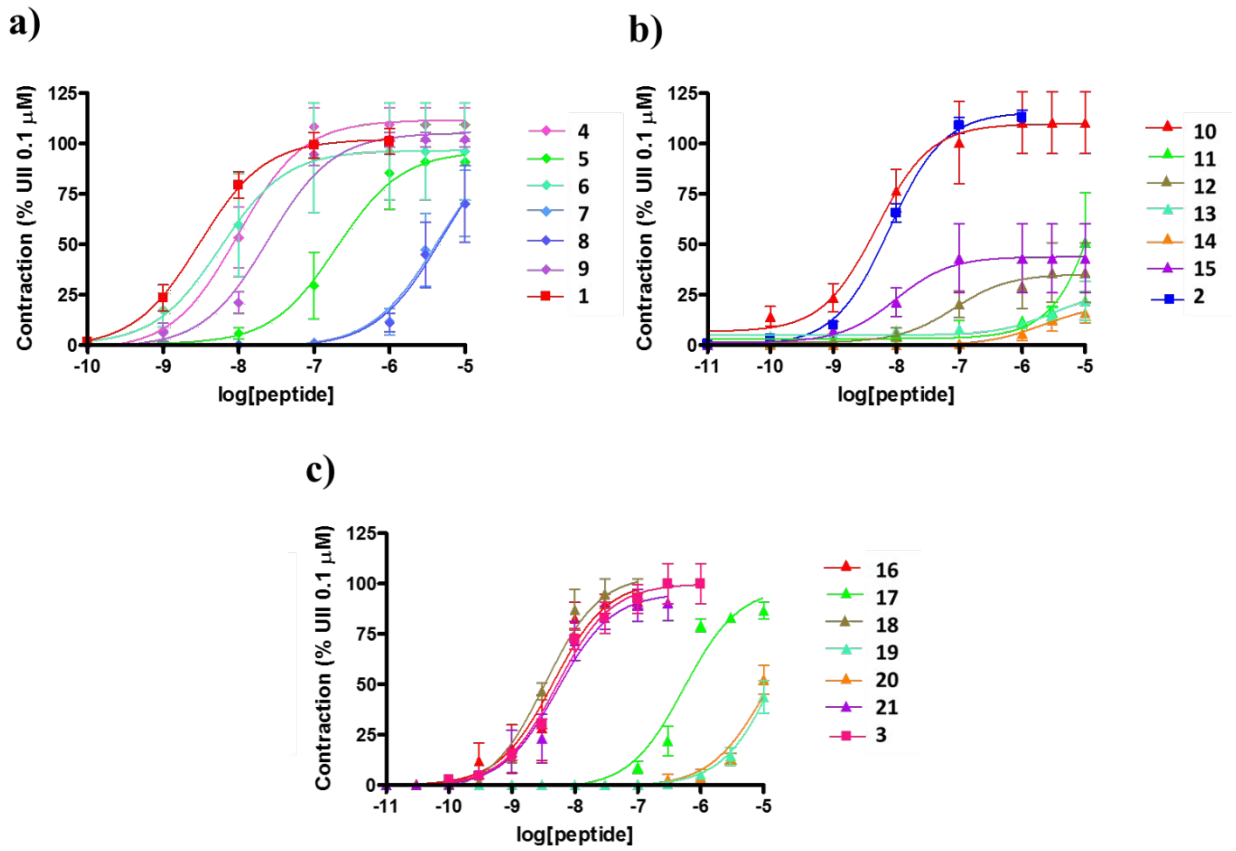

Figure 1. Representative concentration-response curves obtained with rat thoracic aorta rings after adding cumulative concentrations of a) **1** or related *N*-methylated analogs **4-9**; b) **2** or related *N*-methylated analogs **10-15**; c) **3** or related *N*-methylated analogs **16-21**. Efficacy is expressed as a percentage of the KCl-induced contraction (40 mM) divided by the tissue-response induced by **1** (10^{-7} M). Each replicate (n) was conducted on tissue from at least 3 different animals. Data represent the mean ± S.E.M.

Analysis of the contractile potential of *N*-methyl analogs of **2** indicated that the weak binding affinity of *N*-Me-Phe^3 (**11**), *N*-Me-Lys^5 (**13**) and *N*-Me-Tyr^6 (**14**) correlated with inability to induce contractile action on rat aortic ring (Table 2, Figure 1b). Although *N*-methylation at both cysteines of **2** had little impact on binding affinity, *N*-Me-Cys^2 (**10**) was a full agonist and *N*-Me-Cys^7 (**15**) exhibited partial agonism (E_{max} = 44 ± 6%) in the vasocontractile assay. Previously, inversion of the configuration of the two cysteines in **2** had differentially affected both binding affinity and biological activity with more pronounced effects on Cys^7 than Cys^2.[48]

Evaluation of the contractile action of *N*-methyl analogs of **3** revealed a similar correlation between the low binding affinity of the *N*-methyl Phe^6, Lys^8 and Tyr^9 analogs (*e.g.*, **17**, **19** and **20**, Table 2) and weak agonist activity. Previously, *N*-methylation of the Tyr residue in **3** {*e.g.*, [(*N*-Me)Tyr^9]U-II$_{4-11}$, **20**} and replacement of Phe^6 in **3** with the constrained secondary amino acid octahydro-indole-2-carboxylic acid (Oic) were respectively shown to dramatically reduce peptide potency,[49] and both affinity and contractile activity,[34] consistent with perturbation of intra-molecular hydrogen bonds between Phe^6 and Tyr^9 that stabilize the active secondary structure.[46] In contrast, respective *N*-methylation of the amide bonds of Trp and the two Cys

residues in **16**, **18** and **21** led to peptides exhibiting equipotent binding affinity and contractile activity as **3** (Table 2, Figure 1c).

Comparing the effects of *N*-methylation on peptides **1**-**2**, certain positions exhibit divergent activity contingent on the parent structure. For example, *N*-Me-Cys^{10} analogs of **1** and **3** (*e.g.*, **9** and **21**) acted as full agonists, but in their counterpart **2** (*e.g.*, **15**) *N*-methylation resulted in partial agonism (E_{max} = 44 ± 6%). Such differences in the behavior of the two cysteines that belong to **2** were also previously observed with [DCys^2]URP and [DCys^7]URP.[48] Indeed, inversion of configuration of Cys^2 in **2** was less detrimental for the contractile activity than similar replacement of Cys^7,[48] which is also illustrated herein comparing the activities between **10** and **15**. As previously demonstrated, the presence of specific interactions between the *N*-terminal domain of **1** and **3** and UTR might modulate the topography of the binding pocket accommodating the common *C*-terminal tail of the peptides.[35] Hence, as expected, modifications occurring on Cys^{10} in **1** and **3** produce distinct outcomes compared to similar modification in **2**. Finally, our recent works suggested that the orientation of Tyr$^{6/9}$ side chain in **2** and **3** may affect the contractile activity of the ligand.[50-52] It is therefore possible that the *N*-methylation of Cys$^{7/10}$ in **1** and **2** may restrict the orientation of the adjacent Tyr residue impacting only on the contractile profile of **2**. Altogether, these results suggest that the conformational requirements of the Tyr residue may differ between **1**, **2** and **3**.

Moreover, agonist potency varied with *N*-methylation of the Phe residue: **5** (pEC_{50} 6.70 ± 0.30) > **17** (pEC_{50} 6.36 ± 0.04) >> **11** (pEC_{50} < 5). The Phe amide NH or the conformation of the phenyl ring appear to be more relevant for the activity of **2** than **1** and **3**, therefore suggesting a subtle but different involvement of this residue in UTR activation. Accordingly, substitution of the phenylalanine residue with a cyclohexylalanine moiety (Cha) in **3** was reported to generate

an inactive analog, *i.e.* [Cha^6]U-II$_{4-11}$,[53] that suppressed the vasoconstrictor effect of **1** on rat aortic rings. The same modification of **2**, *i.e.* [Cha^3]URP, produced a partial agonist.[53] Moreover, introduction of iodide at the *para* position of the phenyl ring of Phe in **2** and **3** led to divergent vasoconstrictor activities: [Phe(*p*I)^3]URP acted as a partial agonist and [Phe(*p*I)^6]U-II$_{4-11}$ behaved as a full agonist.[54] As recently reported, interaction between Asp^4 of **1** and **3** with Arg^{193} of UTR may influence the positioning of TM4 and ECL2 of UTR, two domains whose flexibility is crucial for receptor activation upon ligand binding.[54] Importantly, these two domains delineate the binding site of the Phe$^{3/6}$ residue.[55] Hence, the absence of interaction in the case of **2**, in which the Asp^4 residue is replaced by an alanine, will therefore create a slightly different binding pocket that might otherwise accommodate this residue, so explaining the difference of contractile activity between **2** and **3** Phe-substituted analogues despite retaining similar affinity.[54]

N-Methylation of Trp^4 of **2** in **12** led also to a partial agonist (E_{max} = 35 ± 5*** %) in contrast to agonists **6** and **18**. Previously, enantiomeric substitution of DTrp for Trp in both **1** and **2** provided [DTrp^7]*h*U-II, which had a 100 fold lower affinity for UTR than **1** and acted as a partial agonist,[33] and [DTrp^4]URP, which exhibited high affinity and completely abolished the rat aortic ring contraction induced by **1**.[48] Accordingly, similar results were obtained elsewhere.[32,33] Considering the divergent behavior of Trp analogs of **1** and **2**, allosteric modulators were developed by substitution of alternative residues at this particular residue in **2** and **3**.[39,56,57] To resume, *N*-methyl substitution of residues Phe$^{3/6}$, Trp$^{4/7}$ and Cys$^{7/10}$ resulted in divergent effects in peptides **1**-**3** highlighting the relevance of their backbone amides for affinity and activity.

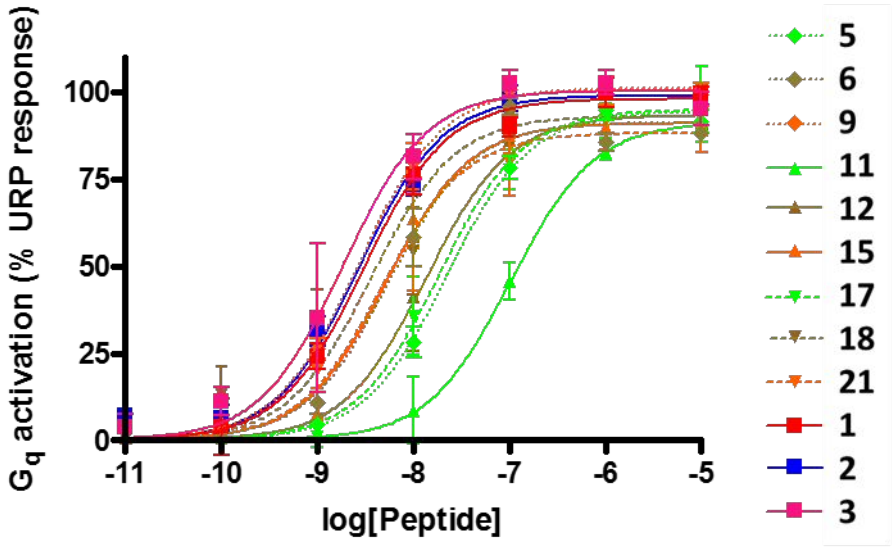

Figure 2. Representative concentration-response curves of G_q protein activation for peptides, **5**, **6**, **9**, **11**, **12**, **15**, **17**, **18**, **21** and **1**, **2**, **3** using a BRET-based biosensor. Efficacy is expressed as a percentage of the activation induced by **2** (10^{-5} M). Each replicate (n) was conducted on at least 3 different cellular passages. Data represent the mean ± S.E.M.

Table 3. G_q activation of **1**, **2**, **3** and selected analogs **5**, **6**, **9**, **11**, **12**, **15**, **17**, **18**, and **21**.

Peptide	*G_q activation*		
	pEC_{50}[a]		**E_{max}**[b]
URP (**2**)	8.57 ± 0.08	N.S.	100 ± 3
U-II_{4-11} (**3**)	8.73 ± 0.14	N.S.	100 ± 4
*h*U-II (**1**)	8.52 ± 0.09		98 ± 3
[(*N*-Me)Phe^3]URP (**11**)	6.98 ± 0.17***	#	91 ± 7
[(*N*-Me)Phe^6]U-II_{4-11} (**17**)	7.73 ± 0.13**	N.S.	95 ± 5
[(*N*-Me)Phe^6]*h*U-II (**5**)	7.65 ± 0.05***		95 ± 5
[(*N*-Me)Trp^4]URP (**12**)	7.86 ± 0.15***	#	93 ± 5
[(*N*-Me)Trp^7]U-II_{4-11} (**18**)	8.44 ± 0.17	N.S.	94 ± 5

[(*N*-Me)Trp^{7}]*h*U-II (**6**)	8.25 ± 0.08		91 ± 3
[(*N*-Me)Cys^{7}]URP (**15**)	8.28 ± 0.10	N.S.	91 ± 3
[(*N*-Me)Cys^{10}]U-II$_{4\text{-}11}$ (**21**)	8.33 ± 0.15	N.S. N.S.	89 ± 4
[(*N*-Me)Cys^{10}]*h*U-II (**9**)	8.57 ± 0.05		101 ± 5

[a]pEC$_{50}$: –log EC$_{50}$; [b]Maximum efficacy is expressed as a percentage of the amplitude of the activation induced by **2** (10^{-5} M). All values are expressed as mean ± S.E.M. Statistical analysis was performed using an unpaired Student's t test, *$P \leq 0.05$, **$P \leq 0.01$, ***$P \leq 0.001$, *versus* values obtained for non-*N*-methylated-peptide (either **1**, **2** or **3**); # $P \leq 0.05$, comparing the isoforms sharing the same modification. Each replicate (n) was conducted on different cellular passage. N.S.: non significant.

Activation of G_q was associated with aortic contraction mediated by **1** and **2**.[58] The influence of *N*-methylation at the Phe$^{3/6}$, Trp$^{4/7}$ and Cys$^{7/10}$ residues on G_q activation was thus investigated in a comparison of the nine *N*-methyl analogs (**5**, **6**, **9**, **11**, **12**, **15**, **17**, **18**, and **21**) to peptides **1**-**3**. The latter three reference peptides **1**-**3** activated G_q with similar potency and efficacy (Table 3, Figure 2). *N*-Methylation had a limited influence that usually reduced agonist potency to activate G_q. At the Phe residue, this resulted in weak agonists, but **11** appeared to be significantly weaker than **5** and **17**, which was consistent with their affinities and contractile activities. *N*-Methylation of Trp in **2** led to a significantly weaker agonist (**12**) compared to **6** and **18**, which appeared to be equally active as their parent peptides, consistent with their aortic activities. *N*-Methylation of Cys^{7} impacted however the contractile activity of **2** without affecting **1** and **3**, which activated G_q with the same potency as their parent peptides. In contrast to analogs of **1**, **9** and **21**, an analog of **2**, **15**, may activate another pathway involved in aortic contraction, perhaps the small GTPase RhoA through G_{12} activation contributing to aortic ring contraction mediated by **1**.[59] Although activation of G_{12} was not examined, the present results suggest that **15** and potentially the partial

contractile agonist **12** behave as biased agonists. For reference, biased agonists have previously been produced on substitution of Phe[3] and Tyr[6] of **2**.[50,54]

Conformational analysis by NMR spectroscopy. Previously, NMR spectroscopy supported with computational analysis demonstrated that the amide NH and CO moieties of Phe[6] and Tyr[9] engaged in two hydrogen bonds that stabilized a *β*-hairpin conformation in peptides **1**-**3**.[46,47,51,52,61,62] Consistently, *N*-methylation of the Phe[6] and Tyr[9] amides reduced binding affinity and activity in the different analogs. In contrast, spectroscopic analysis of peptides **1**-**3** has not implicated the Lys amide in intramolecular hydrogen bonding,[46,47] yet *N*-Me-Lys derivatives **7**, **13** and **19**, all lost affinity and potency. To examine the latter effect of *N*-methylation, [(*N*-Me)Lys[8]]U-II$_{4\text{-}11}$ (**19**) was investigated by NMR spectroscopy in SDS micelles in solution.[46] The improved affinity and activity of [(*N*-Me)Trp[7]]U-II$_{4\text{-}11}$ (**18**) relative to **3** also required a conformational analysis. Considering that *N*-methylation of the Trp and Lys amides had limited influence on binding of peptides **1**-**3**, and that the three latter peptides adopted similar conformations at their cyclic regions in earlier NMR studies,[35,46] the results of the spectroscopic analyses of *N*-methyl peptides **18** and **19** may be used to interpret the effects of similar modifications on their respective **1** and **2** homologues (*e.g.*, **6**, **12**, and **7**, **13**). Peptides **18** and **19** and their parent **3**, here reported for comparison,[46] exhibited similar NMR spectra (Tables S2-S4, see Supporting Information), which indicate the presence of a *β*-hairpin structure centered on the Trp[7] and Lys[8] residues. Mainly, medium range NOE signals demonstrated the presence of this structural feature (Tables S5-S6, see Supporting Information). The NMR spectrum of [(*N*-Me)Trp[7]]U-II$_{4\text{-}11}$ (**18**) differed from that of **3** by intense downfield shifts of the Hα resonances of residues 4-6 and 9-11, which flank the central turn (Figure S11, see Supporting Information), and

indicated that methylation at Trp^7 caused hairpin stabilization. Significant up-field shifts of the NH and Hγ resonances of Lys^8 and the Hα signal of Trp^7, due to the ring current of the indole moiety, indicated stabilization of the *trans* χ_1-dihedral angle orientation of the Trp^7 side chain. In contrast, in the spectrum of [(*N*-Me)Lys^8]U-II$_{4\text{-}11}$ (**19**), the Hα resonances of Trp^7 and Lys^8 exhibited large downfield shifts compared to those of random coil peptides indicative of a conformational change at the turn region (Figure S11).[63] Computational analysis using molecular dynamics (MD) and NMR-derived constraints (Tables S5-S6, see Supporting Information) provided an ensemble of conformations for each peptide, from which the ten lowest energy conformers were grouped together (Figure 3).

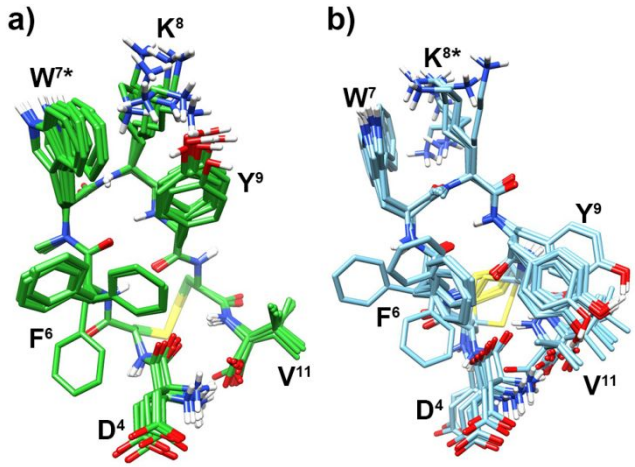

Figure 3. Superposition of the ten lowest energy conformers of a) **18** (PDB code: 6HVB) and b) **19** (PDB code: 6HVC). Structures were superimposed using the backbone heavy atoms of residues 5-10. Heavy atoms are shown with different colors (carbon, green or cyan; nitrogen, blue; oxygen, red; sulfur, yellow). Only polar hydrogen atoms are shown for clarity. A star indicates the *N*-methylated residues.

A well-defined *β*-hairpin structure was observed for peptide **18** having a rms deviation of the cyclic backbone heavy atoms equal to 0.10 Å (Figure 3a). The ensemble of NMR-derived conformers of peptide **18** was significantly better defined than that previously obtained for **3** (rmsd 0.22 Å).[46] The slight yet significant improvement of both the affinity and activity of peptide **18** compared to **3** may tentatively be attributed to stabilization of this conformation.

A similar stabilization of the *β*-hairpin conformer for [(*N*-Me)Trp^4]URP (**12**) may account for the improved binding affinity compared to **2**. The reduced potency and efficacy of **12** may be due to the loss of flexibility of the Trp^7 side chain, which is forced into a *trans* conformation to avoid a steric clash with the *N*-methyl amide. UTR activation by **2** may thus require a post-binding movement of the Trp^7 side chain, which is inhibited in **12**. Considering both [(*N*-Me)Trp^7]*h*U-II (**6**) and [(*N*-Me)Trp^7]U-II$_{4\text{-}11}$ (**18**) exhibited increased binding affinity and potency compared to their parent peptides **1** and **3**, adjustment of the Trp^7 side chain may not be necessary for their activation of the UTR, in contrast to **2**. Accordingly, constraint of the Trp side chain to a *gauche*-(+) or *trans* orientation by cyclization onto the nitrogen of the *C*-terminal Lys^5 in a 4-amino-1,2,4,5-tetrahydroindolo[2,3-c]-azepin-3-one residue (Aia) has provided [Aia^4]URP, which exhibited partial agonism in the aortic ring contraction assay.[47]

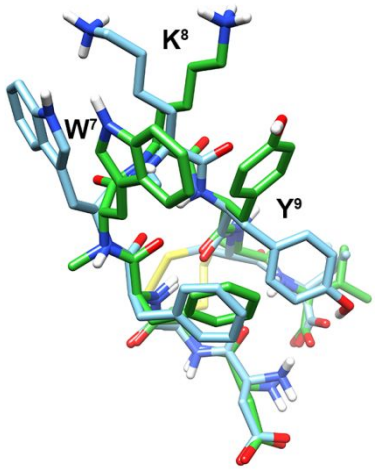

Figure 4. Superposition of the lowest energy conformers of **18** and **19**. Structures were superimposed using the backbone heavy atoms of residues 5-10. Heavy atoms are shown with different colors (carbon, green or cyan; nitrogen, blue; oxygen, red; sulfur, yellow). Only polar hydrogen atoms are shown for clarity.

The *β*-hairpin structure typical of UTR ligands was retained in [(*N*-Me)Lys^8]U-II$_{4-11}$ (**19**, Figure 3b); however significant differences in the orientation of the side chains of Trp^7 and Tyr^9 were observed in comparison with **3** and **18** (Figure 4), due likely to steric clashes between the *N*-methyl amide and the proximal indole and phenol side chains. Although the Trp^7 side chain χ_1 angle was oriented *trans* in both **3** and **19**, the χ_2 angle rotated 60° to −127° in **19**. The Tyr^9 side chain χ_1 angle rotated from a *gauche*-(−) (in **3** and **18**) to a *trans* conformation in **19**. Moreover, the Lys^8 side chain, which is relatively flexible in peptides **3**, **18** and **19**, rotated from a preferred *gauche*-(+) χ_1 angle in **3** and **18** to a preferred *gauche*-(−) orientation in **19** (Figure 4), placing the positively charged nitrogen in a different position. The *trans* orientation of the χ_1 angle of Tyr^9 shown by **19** has been also observed in a few analogs of **3** and suggested to promote antagonism.[52,61,63] Low efficacy of analogs **9**, **15**, and **21** is in accordance with this suggestion. In

contrast, the observed Trp[9] orientation around χ_2 angle in **19** is unprecedented in our studies and may account in part for the drop in affinity and potency of the *N*-Me-Lys[8/5] derivatives **7**, **13** and **19**. In contrast, *N*-methylation of the corresponding lysine residue in octreotide analogs has been well tolerated in certain somatostatin receptors binding ligands that engage sst_2 and sst_5 subtypes.[5,64] Such a structural requirement may account in part for the reciprocal activity of ligands of UTR *vs* somatostatin receptors.

CONCLUSIONS

N-Methylation of peptide backbone amide bonds is commonly used to improve "drug-like" properties of peptides. A new application of this technique has been demonstrated by the *N*-methylation of amides at the cyclic core regions of the two endogenous peptide ligands of UTR. Synthesis and examination of the biological profiles of *N*-methyl-peptides **4-21** of the endogenous peptides **1** and **2** has proven effective to dissect their shared conformer from the different conformational requirements responsible for their distinct activities. Notably, *N*-methylation at the Lys and Tyr residues resulted in a loss of agonist activity of both natural ligands **1** and **2**. The *N*-methylation of the Phe residue of **2** (*e.g.*, **11**) reduced the ability to induce aortic contraction and to activate G_q more significantly compared to the same modification of **1** and **3** (*e.g.*, **5** and **17**, respectively). *N*-Methylation of the Trp residue of **2** (*e.g.*, **12**) enhanced binding affinity, but drastically reduced contractile efficacy and G_q activation potency, in contrast to the same modification on **1** and **3** (*e.g.*, **6** and **18**, respectively). *N*-Methylation of the Cys[7/10] (*e.g.*, **9**, **15** and **21**) had different effects on vasocontractile action without influencing binding affinity of **1**-**3**. Conformational analysis of select analogs (*e.g.*, **18** and **19**) revealed different conformational requirements that may explain the functional selectivity observed

between peptide hormones **1** and **2**. Finally, considering the interest in the urotensinergic system has been renewed in light of the discovery of biased agonism at UTR and an emerging role in inflammatory disease and cancer, our study focused on the *N*-methylation scanning of **1**, **2** and **3** peptide sequences offers, for the first time in this context, tools to discern the specific molecular determinants involved in such functional selectivity.

EXPERIMENTAL SECTION

Materials and general methods. The amino acids Fmoc-Val-OH, Fmoc-Cys(Trt)-OH, Fmoc-Tyr(*t*Bu)-OH, Fmoc-Lys(Boc)-OH, Fmoc-Trp(Boc)-OH, Fmoc-Phe-OH, Fmoc-Asp(O*t*Bu)-OH, Fmoc-Ala-OH, Fmoc-Pro-OH, Fmoc-Thr(*t*Bu)-OH, and Fmoc-Glu(O*t*Bu)-OH, all were purchased from GL Biochem Ltd (Shangai, China). Coupling reagents used, that are *N,N,N',N'*-tetramethyl-*O*-(1*H*-benzotriazol-1-yl)uronium hexafluorophosphate (HBTU), *O*-(7-azabenzotriazol-1-yl)-*N,N,N',N'*-tetramethyluronium hexafluorophosphate (HATU), 1-hydroxybenzotriazole (HOBt), and 1-hydroxyazabenzotriazole (HOAt), all were also obtained commercially from GL Biochem Ltd (Shangai, China). The Wang resin (0.64 mmol/g as loading) was purchased from Chem-Impex, and the manufacturer's reported loading of the resin was used in the calculation of final product yields. *N,N*-diisopropylethylamine (DIEA), acetic anhydride, 4-(dimethylamino)pyridine (DMAP), *orto*-nitrobenzenesulfonyl (*o*-NBS) chloride, 2,4,6-collidine, DIAD, Ph_3P, 2-mercaptoethanol, anisole, dimethyl sulfoxide (DMSO), all were purchased from Sigma-Aldrich/Merck and used as received. Piperidine, trifluoroacetic acid (TFA) and DBU, were purchased from Iris Biotech GmbH. Solvents for peptide synthesis such as *N,N*-dimethylformamide (DMF), dichloromethane (DCM), NMP, diethyl ether (Et_2O), and for HPLC analyses and purifications such as water, MeOH and acetonitrile (MeCN), were reagent

grade acquired from commercial sources (Merck/Sigma-Aldrich and VWR) and used without further purification. Anhydrous solvents [DCM, DMF and tetrahydrofuran (THF)] were obtained by Merck/Sigma Aldrich. LC-MS analyses were performed on a LC-MS instrument from Agilent Technologies equipped with an analytical C18 column (Phenomenex Kinetex, 5 μm, 150 mm × 4.6 mm, 100 Å) and 6110 Quadrupole, in positive electrospray ionization (ESI) mode, to confirm *N*-methylation step and difficult couplings had achieved >90% conversion. High-resolution mass (HRMS) measurements were recorded on a LTQ Orbitrap mass spectrometer in positive ESI mode, and proton adducts $[M + H]^+$ were used for empirical formula confirmation.

Purification of compounds **4-21** was performed on a semi-preparative reverse-phase C18 column (Phenomenex Kinetex, 5 μm, 150 × 21.2 mm, 100 Å) using specific linear gradients of MeCN (0.1% TFA) in water (0.1% TFA) with a flow rate of 10 mL/min (from 10 to 90% over 40 min) and UV detection at 220 nm. Final products were obtained by freeze-drying the appropriate fractions after removal of MeCN under reduced pressure by rotary evaporation. The purity of compounds **4-21** was ascertained using analytical HPLC analyses, which were performed on a reverse-phase C18 column (Phenomenex Kinetex, 5 μm, 150 mm × 4.6 mm, 100 Å) with a flow rate of 1 mL/min using a gradient of MeCN (0.1% TFA) or MeOH (0.1% TFA) in water (0.1% TFA), and UV detection at 220 and 254 nm. All compounds examined for biological activity were purified to >98%, and the correct molecular ions were confirmed by HRMS (Table S1, see Supporting Information).

Synthesis of protected linear sequences. The synthesis of *N*-methylated analogs **4-21** was performed manually in a stepwise fashion by SPPS,[38,39,65] using Fmoc/*t*Bu orthogonal protection. Wang resin (0.2 mmol) was placed into a 10-mL plastic syringe tube equipped with Teflon™

filter, stopper, and stopcock, pre-swollen in DMF on an automated shaker at rt for 30 min, treated with the first amino acid, Fmoc-Val-OH (4 equiv), HBTU (4 equiv), HOBt (4 equiv), DIEA (8 equiv) and a catalytic amount of DMAP (0.15 equiv), to facilitate ester formation, all suspended in DMF, and shaken for 3 h, at rt. After the reaction was ascertained to have gone to completion, the resin was washed with DMF (2 mL × 3) and DCM (2 mL × 3). To avoid potential parallel synthesis of side products, any remaining reactive resin sites were end capped by treatment with acetic anhydride (2 equiv), DIEA (4 equiv) and DMAP (0.4 equiv) in DCM, and the resulting mixture was agitated for 16 h at rt. The resin was washed with DMF (2 mL × 3) and DCM (2 mL × 3). The N^{α}-Fmoc protecting group was removed from the Val residue by treatment with 20:80 piperidine/DMF (*v/v*) (2 mL × 5 min, 2 mL × 25 min). The resin was washed with DMF (2 mL × 3) and DCM (2 mL × 3). The protected amino acids (4 equiv) needed for the construction of required peptide sequence [Fmoc-Cys(Trt)-OH, Fmoc-Tyr(*t*Bu)-OH, Fmoc-Lys(Boc)-OH, Fmoc-Trp(Boc)-OH, Fmoc-Phe-OH, Fmoc-Asp(O*t*Bu)-OH and Fmoc-Ala-OH] were then coupled according to SPPS protocols,[38] using HBTU (4 equiv) and HOBt (3 equiv) in the presence of DIEA (8 equiv) as base, in DMF for 2 h, at rt. Accordingly, Fmoc protection was removed after amino acid couplings as described above. The resins were washed after each coupling and Fmoc group removal step with DMF (2 mL × 3) and DCM (2 mL × 3). Moreover, the progression of the coupling and Fmoc-deprotection reactions was monitored by the observation of colorimetric tests such as the Kaiser and *p*-chloranil tests for primary and secondary amines, respectively.[66] Ambiguous couplings were confirmed by LC-MS monitoring.

N-Methylation procedure and coupling on secondary amines. *N*-Methylation was performed after coupling and Fmoc-deprotection of the corresponding amino acid in three steps.[4,16,41] First, the amino group was converted to an *o*-nitrobenzene sulfonamide by reaction with *o*-NBS

chloride (5 equiv) and 2,4,6-collidine (10 equiv) in NMP for 15 min at rt. The *N*-methylation was performed under Mitsunobu conditions:[43,44] triphenylphosphine (10 equiv), DIAD (5 equiv) and MeOH (5 equiv), together with the resin, all were suspended in anhydrous THF (4 mL) and shaken at rt for 10 min. Finally, the *o*-NBS group was removed by treatment with 2-mercaptoethanol (10 equiv) and DBU (5 equiv) in NMP for two cycles of 5 min each. This deprotection procedure yielded the corresponding secondary amine, which was detected by the observation of both Kaiser and *p*-chloranil colorimetric tests.[66] Due to the steric hindrance of *N*-methyl amino acids, the next coupling employed HATU (3 equiv) and HOAt (3 equiv) in the presence of DIEA (6 equiv), dissolved in a small volume of NMP (2-3 mL). The reaction was carried out at rt for 16 h and complete coupling was confirmed by LC-MS analysis of the residue after an aliquot of resin (5 mg) was treated with a cleavage cocktail of 95:2.5:2.5 TFA/TIS/H_2O (*v/v/v*) at rt for 1 h, filtered, and evaporated.

Peptide cleavage. After Fmoc group removal as described above, the resin was washed with DMF (2 mL × 3) and DCM (2 mL × 3) and dried *in vacuo*. Then, peptide was released from the solid support, protecting groups were removed, and, simultaneously, the disulfide bridge was formed, by treating the resin with a solution of 89:10:1 TFA/DMSO/anisole (*v/v/v*) at rt for 3 h. The resin was filtered and washed with a small amount of fresh TFA. The combined filtrate was precipitated in chilled diethyl ether, stored at −6 °C for 15 min, and centrifuged to yield crude peptide as pale yellow pellet, which was purified by HPLC to afford the respective peptide (**4-21**) as white powder.

[(*N*-Me)Cys^5]*h*U-II (**4**) - purity >98%; t_R = 15.5 min [analytical HPLC/Gradient#1, isocratic 10% MeCN (0.1% TFA) in H_2O (0.1% TFA) over 5 min, and gradient 10-90% MeCN (0.1% TFA) in H_2O (0.1% TFA) over 20 min, flow rate of 1.0 mL/min], and t_R = 24.7 min

[analytical HPLC/Gradient#2, isocratic 10% MeOH (0.1% TFA) in H_2O (0.1% TFA) over 5 min, and gradient 10-90% MeOH (0.1% TFA) in H_2O (0.1% TFA) over 20 min, flow rate of 1.0 mL/min]; HRMS (ESI) *m*/*z* calculated for molecular formula $C_{65}H_{88}N_{13}O_{18}S_2^+$ $[M + H]^+$ 1402.5812, found 1402.5681.

[(*N*-Me)Phe^6]*h*U-II (5) - purity >98%; t_R = 15.2 min [analytical HPLC/Gradient#1, isocratic 10% MeCN (0.1% TFA) in H_2O (0.1% TFA) over 5 min, and gradient 10-90% MeCN (0.1% TFA) in H_2O (0.1% TFA) over 20 min, flow rate of 1.0 mL/min], and t_R = 21.5 min [analytical HPLC/Gradient#2, isocratic 10% MeOH (0.1% TFA) in H_2O (0.1% TFA) over 5 min, and gradient 10-90% MeOH (0.1% TFA) in H_2O (0.1% TFA) over 20 min, flow rate of 1.0 mL/min]; HRMS (ESI) *m*/*z* calculated for molecular formula $C_{65}H_{88}N_{13}O_{18}S_2^+$ $[M + H]^+$ 1402.5812, found 1402.5831.

[(*N*-Me)Trp^7]*h*U-II (6) - purity >98%; t_R = 16.4 min [analytical HPLC/Gradient#1, isocratic 10% MeCN (0.1% TFA) in H_2O (0.1% TFA) over 5 min, and gradient 10-90% MeCN (0.1% TFA) in H_2O (0.1% TFA) over 20 min, flow rate of 1.0 mL/min], and t_R = 24.3 min [analytical HPLC/Gradient#2, isocratic 10% MeOH (0.1% TFA) in H_2O (0.1% TFA) over 5 min, and gradient 10-90% MeOH (0.1% TFA) in H_2O (0.1% TFA) over 20 min, flow rate of 1.0 mL/min]; HRMS (ESI) *m*/*z* calculated for molecular formula $C_{65}H_{88}N_{13}O_{18}S_2^+$ $[M + H]^+$ 1402.5812, found 1402.5983.

[(*N*-Me)Lys^8]*h*U-II (7) - purity >98%; t_R = 14.8 min [analytical HPLC/Gradient#1, isocratic 10% MeCN (0.1% TFA) in H_2O (0.1% TFA) over 5 min, and gradient 10-90% MeCN (0.1% TFA) in H_2O (0.1% TFA) over 20 min, flow rate of 1.0 mL/min], and t_R = 21.2 min [analytical HPLC/Gradient#2, isocratic 10% MeOH (0.1% TFA) in H_2O (0.1% TFA) over 5 min, and gradient 10-90% MeOH (0.1% TFA) in H_2O (0.1% TFA) over 20 min, flow rate of 1.0

mL/min]; HRMS (ESI) *m*/*z* calculated for molecular formula $C_{65}H_{88}N_{13}O_{18}S_2^+$ [M + H]$^+$ 1402.5812, found 1402.5934.

[(*N*-Me)Tyr^9]*h*U-II (**8**) - purity >98%; t_R = 15.0 min [analytical HPLC/Gradient#1, isocratic 10% MeCN (0.1% TFA) in H_2O (0.1% TFA) over 5 min, and gradient 10-90% MeCN (0.1% TFA) in H_2O (0.1% TFA) over 20 min, flow rate of 1.0 mL/min], and t_R = 21.2 min [analytical HPLC/Gradient#2, isocratic 10% MeOH (0.1% TFA) in H_2O (0.1% TFA) over 5 min, and gradient 10-90% MeOH (0.1% TFA) in H_2O (0.1% TFA) over 20 min, flow rate of 1.0 mL/min]; HRMS (ESI) *m*/*z* calculated for molecular formula $C_{65}H_{88}N_{13}O_{18}S_2^+$ [M + H]$^+$ 1402.5812, found 1402.5861.

[(*N*-Me)Cys^{10}]*h*U-II (**9**) - purity >98%; t_R = 15.8 min [analytical HPLC/Gradient#1, isocratic 10% MeCN (0.1% TFA) in H_2O (0.1% TFA) over 5 min, and gradient 10-90% MeCN (0.1% TFA) in H_2O (0.1% TFA) over 20 min, flow rate of 1.0 mL/min], and t_R = 23.3 min [analytical HPLC/Gradient#2, isocratic 10% MeOH (0.1% TFA) in H_2O (0.1% TFA) over 5 min, and gradient 10-90% MeOH (0.1% TFA) in H_2O (0.1% TFA) over 20 min, flow rate of 1.0 mL/min]; HRMS (ESI) *m*/*z* calculated for molecular formula $C_{65}H_{88}N_{13}O_{18}S_2^+$ [M + H]$^+$ 1402.5812, found 1402.5928.

[(*N*-Me)Cys^2]URP (**10**) - purity >98%; t_R = 15.7 min [analytical HPLC/Gradient#1, isocratic 10% MeCN (0.1% TFA) in H_2O (0.1% TFA) over 5 min, and gradient 10-90% MeCN (0.1% TFA) in H_2O (0.1% TFA) over 20 min, flow rate of 1.0 mL/min], and t_R = 23.1 min [analytical HPLC/Gradient#2, isocratic 10% MeOH (0.1% TFA) in H_2O (0.1% TFA) over 5 min, and gradient 10-90% MeOH (0.1% TFA) in H_2O (0.1% TFA) over 20 min, flow rate of 1.0 mL/min]; HRMS (ESI) *m*/*z* calculated for molecular formula $C_{50}H_{67}N_{10}O_{10}S_2^+$ [M + H]$^+$ 1031.4478, found 1031.4493.

[(*N*-Me)Phe^3]URP (11) - purity >98%; t_R = 15.2 min [analytical HPLC/Gradient#1, isocratic 10% MeCN (0.1% TFA) in H_2O (0.1% TFA) over 5 min, and gradient 10-90% MeCN (0.1% TFA) in H_2O (0.1% TFA) over 20 min, flow rate of 1.0 mL/min], and t_R = 21.4 min [analytical HPLC/Gradient#2, isocratic 10% MeOH (0.1% TFA) in H_2O (0.1% TFA) over 5 min, and gradient 10-90% MeOH (0.1% TFA) in H_2O (0.1% TFA) over 20 min, flow rate of 1.0 mL/min]; HRMS (ESI) *m*/*z* calculated for molecular formula $C_{50}H_{67}N_{10}O_{10}S_2^+$ $[M + H]^+$ 1031.4483, found 1031.4470.

[(*N*-Me)Trp^4]URP (12) - purity >98%; t_R = 16.8 min [analytical HPLC/Gradient#1, isocratic 10% MeCN (0.1% TFA) in H_2O (0.1% TFA) over 5 min, and gradient 10-90% MeCN (0.1% TFA) in H_2O (0.1% TFA) over 20 min, flow rate of 1.0 mL/min], and t_R = 24.8 min [analytical HPLC/Gradient#2, isocratic 10% MeOH (0.1% TFA) in H_2O (0.1% TFA) over 5 min, and gradient 10-90% MeOH (0.1% TFA) in H_2O (0.1% TFA) over 20 min, flow rate of 1.0 mL/min]; HRMS (ESI) *m*/*z* calculated for molecular formula $C_{50}H_{67}N_{10}O_{10}S_2^+$ $[M + H]^+$ 1031.4483, found 1031.4496.

[(*N*-Me)Lys^5]URP (13) - purity >98%; t_R = 14.8 min [analytical HPLC/Gradient#1, isocratic 10% MeCN (0.1% TFA) in H_2O (0.1% TFA) over 5 min, and gradient 10-90% MeCN (0.1% TFA) in H_2O (0.1% TFA) over 20 min, flow rate of 1.0 mL/min], and t_R = 21.4 min [analytical HPLC/Gradient#2, isocratic 10% MeOH (0.1% TFA) in H_2O (0.1% TFA) over 5 min, and gradient 10-90% MeOH (0.1% TFA) in H_2O (0.1% TFA) over 20 min, flow rate of 1.0 mL/min]; HRMS (ESI) *m*/*z* calculated for molecular formula $C_{50}H_{67}N_{10}O_{10}S_2^+$ $[M + H]^+$ 1031.4483, found 1031.4509.

[(*N*-Me)Tyr^6]URP (14) - purity >98%; t_R = 14.9 min [analytical HPLC/Gradient#1, isocratic 10% MeCN (0.1% TFA) in H_2O (0.1% TFA) over 5 min, and gradient 10-90% MeCN

(0.1% TFA) in H_2O (0.1% TFA) over 20 min, flow rate of 1.0 mL/min], and t_R = 21.0 min [analytical HPLC/Gradient#2, isocratic 10% MeOH (0.1% TFA) in H_2O (0.1% TFA) over 5 min, and gradient 10-90% MeOH (0.1% TFA) in H_2O (0.1% TFA) over 20 min, flow rate of 1.0 mL/min]; HRMS (ESI) *m*/*z* calculated for molecular formula $C_{50}H_{67}N_{10}O_{10}S_2^+$ $[M + H]^+$ 1031.4483, found 1031.4505.

[(*N*-Me)Cys^7]URP (**15**) - purity >98%; t_R = 16.0 min [analytical HPLC/Gradient#1, isocratic 10% MeCN (0.1% TFA) in H_2O (0.1% TFA) over 5 min, and gradient 10-90% MeCN (0.1% TFA) in H_2O (0.1% TFA) over 20 min, flow rate of 1.0 mL/min], and t_R = 23.5 min [analytical HPLC/Gradient#2, isocratic 10% MeOH (0.1% TFA) in H_2O (0.1% TFA) over 5 min, and gradient 10-90% MeOH (0.1% TFA) in H_2O (0.1% TFA) over 20 min, flow rate of 1.0 mL/min]; HRMS (ESI) *m*/*z* calculated for molecular formula $C_{50}H_{67}N_{10}O_{10}S_2^+$ $[M + H]^+$ 1031.4483, found 1031.4506.

[(*N*-Me)Cys^5]U-II$_{4-11}$ (**16**) - purity >98%; t_R = 15.4 min [analytical HPLC/Gradient#1, isocratic 10% MeCN (0.1% TFA) in H_2O (0.1% TFA) over 5 min, and gradient 10-90% MeCN (0.1% TFA) in H_2O (0.1% TFA) over 20 min, flow rate of 1.0 mL/min], and t_R = 22.6 min [analytical HPLC/Gradient#2, isocratic 10% MeOH (0.1% TFA) in H_2O (0.1% TFA) over 5 min, and gradient 10-90% MeOH (0.1% TFA) in H_2O (0.1% TFA) over 20 min, flow rate of 1.0 mL/min]; HRMS (ESI) *m*/*z* calculated for molecular formula $C_{51}H_{67}N_{10}O_{12}S_2^+$ $[M + H]^+$ 1075.4381, found 1075.4438.

[(*N*-Me)Phe^6]U-II$_{4-11}$ (17) - purity >98%; t_R = 15.2 min [analytical HPLC/Gradient#1, isocratic 10% MeCN (0.1% TFA) in H_2O (0.1% TFA) over 5 min, and gradient 10-90% MeCN (0.1% TFA) in H_2O (0.1% TFA) over 20 min, flow rate of 1.0 mL/min], and t_R = 21.3 min [analytical HPLC/Gradient#2, isocratic 10% MeOH (0.1% TFA) in H_2O (0.1% TFA) over 5 min,

and gradient 10-90% MeOH (0.1% TFA) in H_2O (0.1% TFA) over 20 min, flow rate of 1.0 mL/min]; HRMS (ESI) *m*/*z* calculated for molecular formula $C_{51}H_{67}N_{10}O_{12}S_2^+$ $[M + H]^+$ 1075.4381, found 1075.4426.

[(*N*-Me)Trp^7]U-II$_{4-11}$ (18) - purity >98%; t_R = 16.6 min [analytical HPLC/Gradient#1, isocratic 10% MeCN (0.1% TFA) in H_2O (0.1% TFA) over 5 min, and gradient 10-90% MeCN (0.1% TFA) in H_2O (0.1% TFA) over 20 min, flow rate of 1.0 mL/min], and t_R = 24.2 min [analytical HPLC/Gradient#2, isocratic 10% MeOH (0.1% TFA) in H_2O (0.1% TFA) over 5 min, and gradient 10-90% MeOH (0.1% TFA) in H_2O (0.1% TFA) over 20 min, flow rate of 1.0 mL/min]; HRMS (ESI) *m*/*z* calculated for molecular formula $C_{51}H_{67}N_{10}O_{12}S_2^+$ $[M + H]^+$ 1075.4381, found 1075.4431.

[(*N*-Me)Lys^8]U-II$_{4-11}$ (19) - purity >98%; t_R = 14.7 min [analytical HPLC/Gradient#1, isocratic 10% MeCN (0.1% TFA) in H_2O (0.1% TFA) over 5 min, and gradient 10-90% MeCN (0.1% TFA) in H_2O (0.1% TFA) over 20 min, flow rate of 1.0 mL/min], and t_R = 21.2 min [analytical HPLC/Gradient#2, isocratic 10% MeOH (0.1% TFA) in H_2O (0.1% TFA) over 5 min, and gradient 10-90% MeOH (0.1% TFA) in H_2O (0.1% TFA) over 20 min, flow rate of 1.0 mL/min]; HRMS (ESI) *m*/*z* calculated for molecular formula $C_{51}H_{67}N_{10}O_{12}S_2^+$ $[M + H]^+$ 1075.4381, found 1075.4409.

[(*N*-Me)Tyr^9]U-II$_{4-11}$ (20) - purity >98%; t_R = 14.9 min [analytical HPLC/Gradient#1, isocratic 10% MeCN (0.1% TFA) in H_2O (0.1% TFA) over 5 min, and gradient 10-90% MeCN (0.1% TFA) in H_2O (0.1% TFA) over 20 min, flow rate of 1.0 mL/min], and t_R = 21.0 min [analytical HPLC/Gradient#2, isocratic 10% MeOH (0.1% TFA) in H_2O (0.1% TFA) over 5 min, and gradient 10-90% MeOH (0.1% TFA) in H_2O (0.1% TFA) over 20 min, flow rate of 1.0

mL/min]; HRMS (ESI) *m*/*z* calculated for molecular formula $C_{51}H_{67}N_{10}O_{12}S_2^+$ [M + H]$^+$ 1075.4381, found 1075.4387.

[(*N*-Me)Cys^{10}]U-II$_{4-11}$ (21) - purity >98%; t_R = 15.8 min [analytical HPLC/Gradient#1, isocratic 10% MeCN (0.1% TFA) in H_2O (0.1% TFA) over 5 min, and gradient 10-90% MeCN (0.1% TFA) in H_2O (0.1% TFA) over 20 min, flow rate of 1.0 mL/min], and t_R = 23.1 min [analytical HPLC/Gradient#2, isocratic 10% MeOH (0.1% TFA) in H_2O (0.1% TFA) over 5 min, and gradient 10-90% MeOH (0.1% TFA) in H_2O (0.1% TFA) over 20 min, flow rate of 1.0 mL/min]; HRMS (ESI) *m*/*z* calculated for molecular formula $C_{51}H_{67}N_{10}O_{12}S_2^+$ [M + H]$^+$ 1075.4381, found 1075.4415.

Aortic ring contraction experiments. Adult male Sprague-Dawley rats (Charles-Rivers, San Diego, CA) weighing 250-300 g were housed in group cages under controlled illumination (12:12h light-dark cycle), humidity, and temperature (21-23 °C) and given free access to tap water and rat chow. All experimental procedures were performed in accordance with regulations and ethical guidelines from the Canadian Council for the Care of Laboratory Animals and received approvals of the institutional animal care and use committee of the *Institut National de la Recherche Scientifique-Institut Armand-Frappier*. As previously described,[50] the thoracic aorta was cleared of surrounding tissue and then excised from the aortic arch to the diaphragm. Conjunctive tissues were next removed from the thoracic aorta and the vessels were divided into 4 mm rings. The endothelium of each aortic ring was removed by gently rubbing the vessel intimal surface. Aortic rings were then placed in a 5-mL organ bath filled with oxygenated normal Krebs-Henselheit buffer. 80 μL of a 2.5 M KCl solution (40 mM final concentration in bath) was used to evaluate contractile responses of each vessel. In one bath, **1** (10^{-7} M) was

applied as a control, and the tissue-response was expressed as the ratio with the KCl-induced contraction. Cumulative concentration-response curves to synthetic peptides were obtained by increasing the concentration of each peptide in the organ chamber (10^{-11} to 10^{-5} M). The contractile amplitude induced by each concentration of peptide was expressed as a percentage of the KCl-induced contraction divided by the tissue-response induced by **1**. The mean effective concentrations (EC_{50}) are expressed as the mean ± S.E.M., and the *n* values, representing the total number of animals from which the vessels were isolated, varied from 3-19 animals.

Ligand binding. Synthetic **1** or **2** was radiolabeled with $Na^{125}I$ using the chloramine T technique as previously reported.[48] Iodinated ^{125}I-URP or ^{125}I-*h*UII were purified on a C_{18} cartridge, collected and stored at −20 ºC until use. Competition binding experiments were performed using a stable HEK 293-UTR cell line, expressing the human UTR isoform.[50] Cells plated in 96-well plate at a density of 10,000 cells/well were incubated on ice and for 2 h with increasing concentration of various peptides (10^{-11} to 10^{-5} M) in the presence of ^{125}I-URP or ^{125}I-*h*U-II (0.05 nM). Non-specific binding was established by exposing cells to 10^{-5} M cold **1** or **2**. Cells were washed twice with cold binding buffer then lysed with a solution of NaOH (1 M). Cell-bound radioactivity was quantified using a γ-counter. Results were expressed as a percentage of the specific binding of ^{125}I-URP or ^{125}I-*h*U-II obtained in the absence of competitive ligands. Each experiment was performed in triplicate and was conducted on at least three different cellular passages. The mean inhibitory concentrations (IC_{50}) are expressed as the mean ± S.E.M.

G_q activation assays. HEK 293-UTR cells were grown in DMEM culture media supplemented with 10% fetal bovine serum, and G418 (400 μg/mL). Passages were performed when cells

reached 80% of confluency. A transfection mix (1 mL) was prepared in OptiMEM by adding 2.5 µg of a G_q-polycistronic BRET biosensor supplemented with an amount of pBlueScript expression vector sufficient to equate 7.5 µg of DNA and 15 µL of TransIT reagent.[67] Next, this mixture was added 30 minutes later to a premixed suspension of 1.5×10^6 cells in DMEM culture media supplemented with 2.5% fetal bovine serum without antibiotics. Cells were then plated in 96-well plates at a density of 15,000 cells/well. 16 h post-transfection, the medium was replaced with DMEM supplemented with 5% FBS, penicillin-streptomycin (100 U/mL) and G418 (400 µg/mL) then cell growth was resumed for another 24 h. Cells were washed with 120 µL PBS solution supplemented with 0.1 % of glucose, and incubated with 80 µL of this solution for 2 h at 37 °C. Then, 10 µL of a 1/20 dilution (diluted before use) of coelenterazine 400A (stock at 1 mM in ethanol) in Krebs, and 10 µL of the 10× appropriate concentration of ligand were sequentially added. The luminescence was evaluated with an Infinite® M1000 PRO. Filters were set at 410 nm and 515 nm for detecting the *Renilla* luciferase II (RlucII, donor) and green fluorescent protein 10 (GFP10, acceptor) light emission, respectively. BRET signals were monitored for 5 min after co-addition of coelenterazine 400A and ligands. BRET ratio was determined by calculating the ratio of the light emitted by GFP10 over the light emitted by the RlucII. BRET signals were normalized to that of **2** (10^{-5} M). Each experiment was performed in triplicate and was conducted on at least three different cellular passages. The mean effective concentrations (EC_{50}) are expressed as the mean ± S.E.M.

Statistical analysis. Aortic contraction assays, radioligand binding and G protein activation experiments were performed at least in triplicate. Data, expressed as mean ± S.E.M., were analyzed with the Prism Software (Graphpad Software, San Diego, CA, USA). Sigmoidal dose-

response fits with variable slope and one-site competition functions were used to determine EC_{50} and IC_{50}, respectively. K_i values were calculated from IC_{50} using the Cheng-Prusoff equation ($K_i = IC_{50} / (1 + [\text{radioligand}] / K_d)$), with [radioligand] = 0.05 nM and $K_d = 0.067 \pm 0.002$ nM for **1** or $K_d = 0.059 \pm 0.007$ nM for **2**. Statistical comparisons were analyzed by the Student's t-test, and differences were considered significant where $*P < 0.05$, $**P < 0.01$ or $***P < 0.001$.

NMR spectroscopy. The 99.9% ^2H_2O solutions were obtained from Aldrich (Milwaukee, USA), 98% DPC-d_{38} solutions were obtained from Cambridge Isotope Laboratories, Inc. (Andover, USA), and [(2,2,3,3-tetradeuterio-3-(trimethylsilanyl)]propionic acid (TSP) was from MSD Isotopes (Montreal, Canada). The samples for NMR spectroscopy were prepared by dissolving the appropriate amount of peptide in 0.54 mL of ^1H_2O (pH 5.5), 0.06 mL of ^2H_2O to obtain a concentration of 2 mM and 200 mM of SDS-d_{25}. NMR spectra were recorded on a Varian INOVA 700 MHz spectrometer equipped with a z-gradient 5 mm triple-resonance probe head. All the spectra were recorded at a temperature of 25 °C. The spectra were calibrated relative to TSP (0.00 ppm) as internal standard. One-dimensional (1D) NMR spectra were recorded in the Fourier mode with quadrature detection. The water signal was suppressed by gradient echo.[68] Two-dimensional (2D) DQF-COSY,[69] TOCSY,[70] and NOESY[71] spectra were recorded in the phase-sensitive mode using the method by States *et al*.[72] Data block sizes were 2048 addresses in t_2 and 512 equidistant t_1 values. Before Fourier transformation, the time domain data matrices were multiplied by shifted $\sin^2$ functions in both dimensions. A mixing time of 70 ms was used for the TOCSY experiments. NOESY experiments were run with mixing times in the range of 50-200 ms. The qualitative and quantitative analyses of DQF-COSY, TOCSY, and NOESY spectra, were obtained using the interactive program package XEASY.[73] The temperature

coefficients of the amide proton chemical shifts were calculated from 1D ^{1}H NMR and 2D TOCSY experiments performed at different temperatures in the range 25-40 °C by means of linear regression.

Complete ^{1}H NMR chemical shift assignments were effectively achieved for peptides **18** and **19** according to the procedure of Wüthrich[74] via the usual systematic application of DQF-COSY, TOCSY, and NOESY experiments with the support of the XEASY software package (Tables S2-S3, see Supporting Information).

Structure calculation. The NOE-based distance restraints were obtained from NOESY spectra of peptides **18** and **19** collected with a mixing time of 100 ms. The NOE cross peaks were integrated with the XEASY program and were converted into upper distance bounds using the CALIBA program incorporated into the program package DYANA.[75] Only NOE derived constraints were considered in the annealing procedures. The restraints applied during the calculations are reported in Tables S5-S6 (see Supporting Information). NMR-derived upper bounds were imposed as semi-parabolic penalty functions with force constants of 4 Kcal mol^{-1} Å^{-2}. A distance maximum force constant of 1000 Kcal/ mol^{-1} Å^{-2} was used. Non-standard *N*-methylated residues were built using the Insight Builder module (Accelrys Software Inc., San Diego). Atomic potentials and charges were assigned using the consistent valence force field (CVFF).[76] The conformational space of **18** and **19** was sampled through 100 cycles of restrained Simulated Annealing (ε = 1r). In Simulated Annealing, the temperature is altered in time increments from an initial temperature to a final temperature by adjusting the kinetic energy of the structure (by rescaling the velocities of the atoms). The following protocol was applied: the system was heated up to 1500 K over 2000 fs (time step = 1.0 fs); the temperature of 1500 K was

applied to the system for 2000 fs (time step = 1.0 fs) with the aim of surmounting torsional barriers; successively, temperature was linearly reduced to 300 K in 1000 fs (time step = 1.0 fs). Resulting conformations were then subjected to restrained Molecular Mechanics (MM) energy minimization within Insight Discover module (ε = 1r) until the maximum RMS derivative was less than 0.001 kcal/Å, using Conjugate Gradient as minimization algorithm. Finally, conformations were subjected to 1000 steps of unrestrained MM Conjugate Gradient energy minimization. From the produced 100 conformations, 10 structures, whose interprotonic distances best fitted NOE derived distances, were chosen (Figure 3).

ASSOCIATED CONTENT

Supporting Information

Synthetic path for the achievement of compounds **1-21**; Analytical data of compounds **4-21**; HPLC chromatograms of selected peptides (**4**, **6**, **9**, **11**, **12**, **15**, **17-19**, **21**); ^{1}H NMR resonance assignments of **3**, **18** and **19** in SDS-d_{25}; NOE derived upper limit constraints of **18** and **19**; secondary shifts of the Hα protons of **3**, **18** and **19**; molecular formula strings (CSV).

Accession Codes

PDB coordinates of **18** (PDB code: 6HVB) and **19** (PDB code: 6HVC).

AUTHOR INFORMATION

Corresponding Authors

*Prof. Paolo Grieco

Email: paolo.grieco@unina.it

Phone: +39 081 678620

*David Chatenet, PhD

Email: david.chatenet@iaf.inrs.ca

Phone: +1 450 687-5010

Present Address

ΩDiSTABiF, Università degli Studi della Campania 'Luigi Vanvitelli', via Vivaldi 43, 81100 Caserta, Italy.

Author Contributions

‡F.M. and E.B. contributed equally.

Funding Sources

The study was supported by Canadian Institutes of Health Research (CIHR) (MOP-142184) and the Natural Sciences and Engineering Research Council of Canada (NSERC) (RGPIN-2015-04848) to D.C.

Notes

The authors declare no competing financial interest.

ACKNOWLEDGMENT

We thank the Canadian Institutes of Health Research (CIHR) and the Natural Sciences and Engineering Research Council of Canada (NSERC) for funding.

ABBREVIATIONS

1D, one-dimensional; 2D, two-dimensional; Aia, 4-amino-1,2,4,5-tetrahydroindolo[2,3-c]-azepin-3-one; BRET, bioluminescence resonance energy transfer; Cha, cyclohexylalanine; DIAD, diisopropyl azodicarboxylate; DIEA, *N,N*-diisopropylethylamine; DMEM, Dulbecco's Modified Eagle's medium; DQF-COSY, double quantum filtered correlated spectroscopy; FBS, foetal bovine serum; GFP10, green fluorescent protein 10; GPCR, G protein-coupled receptor; HATU, *O*-(7-azabenzotriazol-1-yl)-*N,N,N',N'*-tetramethyluronium hexafluorophosphate; HBTU, 2-(1H-benzotriazole-1-yl)-1,1,3,3-tetramethyluronium hexafluorophosphate; HEK 293 cells, Human Embryonic Kidney 293 cells; HOAt, 1-hydroxyazabenzotriazole; HOBt, 1-hydroxybenzotriazole; *h*U-II, human urotensin II; *o*-NBS, *orto*-nitrobenzenesulfonyl; Oic, octahydro-indole-2-carboxylic acid; Phe(*p*I), *para*-iodo-phenylalanine; RlucII, *Renilla* luciferase II; RP-HPLC, reversed-phase high performance liquid chromatography; SPPS, solid-phase peptide synthesis; TOCSY, total correlated spectroscopy; URP, urotensin II-related peptide; UTR, urotensin II receptor.

REFERENCES

1. Di, L. Strategic approaches to optimizing peptide ADME properties. *AAPS J.* **2014**, *17*, 134–143.

2. Otvos, L.; Wade, J. D. Current challenges in peptide-based drug discovery. *Front. Chem.* **2014**, *2*, 62.

3. Goldflam, M.; Ullman, C. G. Recent advances toward the discovery of drug-like peptides de novo. *Front. Chem.* **2015**, *3*, 69.

4. Chatterjee, J.; Gilon, C.; Hoffman, A.; Kessler, H. N-Methylation of peptides: a new perspective in medicinal chemistry. *Acc. Chem. Res.* **2008**, *41*, 1331–1342.

5. Biron, E.; Chatterjee, J.; Ovadia, O.; Langenegger, D.; Brueggen, J.; Hoyer, D.; Schmid, H. A.; Jelinek, R.; Gilon, C.; Hoffman, A.; Kessler, H. Improving oral bioavailability of peptides by multiple N-methylation: somatostatin analogues. *Angew. Chem. Int. Edit.* **2008**, *47*, 2595–2599.

6. White, T. R.; Renzelman, C. M.; Rand, A. C.; Rezai, T.; Mcewen, C. M.; Gelev, V. M.; Turner, R. A.; Linington, R. G.; Leung, S. S. F.; Kalgutkar, A. S.; Bauman, J. N.; Zhang, Y.; Liras, S.; Price, D. A.; Mathiowetz, A. M.; Jacobson, M. P.; Lokey, R. S. On-resin N-methylation of cyclic peptides for discovery of orally bioavailable scaffolds. *Nat. Chem. Biol.* **2011**, *7*, 810–817.

7. Piriou, F.; Lintner, K.; Fermandjian, S.; Fromageot, P.; Khosla, M. C.; Smeby, R. R.; Bumpus, F. M. Amino acid side chain conformation in angiotensin II and analogs: correlated results of circular dichroism and ^{1}H nuclear magnetic resonance. *Proc. Natl. Acad. Sci. USA* **1980**, *77*, 82–86.

8. Kessler, H. Detection of hindered rotation and inversion by NMR spectroscopy. *Angew. Chem. Int. Edit.* **1970**, *9*, 219–235.

9. Snyder, J. P. Probable unimportance of intramolecular hydrogen bonds for determining the secondary structure of cyclic hexapeptides. Roseotoxin B. *J. Am. Chem. Soc.* **1984**, *106*, 2393–2400.

10. Räder, A. F.; Reichart, F.; Weinmüller, M.; Kessler, H. Improving oral bioavailability of cyclic peptides by *N*-methylation. *Bioorgan. Med. Chem.* **2017**, *26*, 2766–2773.

11. Scherer, G.; Kramer, M. L.; Schutkowski, M.; Reimer, U.; Fischer, G. Barriers to rotation of secondary amide peptide bonds. *J. Am. Chem. Soc.* **1998**, *120*, 5568–5574.

12. Kessler, H.; Gratias, R.; Hessler, G.; Gurrath, M.; Müller, G. Conformation of cyclic peptides. Principle concepts and the design of selectivity and superactivity in bioactive sequences by spatial screening. *Pure Appl. Chem.* **1996**, *68*, 1201–1205.

13. Fosgerau, K.; Hoffmann, T. Peptide therapeutics: current status and future directions. *Drug Discov. Today* **2015**, *20*, 122–128.

14. Chatterjee, J.; Rechenmacher, F.; Kessler, H. *N*-Methylation of peptides and proteins: an important element for modulating biological functions. *Angew. Chem. Int. Edit.* **2013**, *52*, 254–269.

15. Räder, A. F. B.; Weinmüller, M.; Reichart, F.; Schumacher-Klinger, A.; Merzbach, S.; Gilon, C.; Hoffman, A.; Kessler, H. Orally active peptides: is there a magic bullet? *Angew. Chem. Int. Edit.* **2018**, *57*, 14414–14438.

16. Doedens, L.; Opperer, F.; Cai, M.; Beck, J. G.; Dedek, M.; Palmer, E.; Hruby, V. J.; Kessler, H. Multiple *N*-methylation of MT-II backbone amide bonds leads to melanocortin receptor subtype hMC1R selectivity: pharmacological and conformational studies. *J. Am. Chem. Soc.* **2010**, *132*, 8115–8128.

17. Cai, M.; Marelli, U. K.; Mertz, B.; Beck, J. G.; Opperer, F.; Rechenmacher, F.; Kessler, H.; Hruby, V. J. Structural insights into selective ligand-receptor interactions leading to receptor inactivation utilizing selective melanocortin 3 receptor antagonists. *Biochemistry* **2017**, *56*, 4201–4209.

18. Smith, J. M.; Hows, J. M.; Gordon-Smith, E. C. Stability of cyclosporin A in human serum. *J. Clin. Pathol.* **1983**, *36*, 41–43.

19. Sterner, O.; Etzel, W.; Mayer, A.; Anke, H. Omphalotin, a new cyclic peptide with potent nematicidal activity from *Omphalotus Olearius* II. Isolation and structure determination. *Nat. Prod. Lett.* **1997**, *10*, 33–38.

20. (a) Shemyakin, M.; Ovchinnikov, Y.; Ivanov, V.; Kiryushkin, A. The structure of enniatins and related antibiotics. *Tetrahedron* **1963**, *19*, 581–591; (b) Bevan, K.; Davies, J. S.; Hall, M. J.; Hassall, C. H.; Morton, R. B.; Phillips, D. A. S.; Ogihara, Y.; Thomas, W. A. The monamycins, a new family of cyclodepsipeptide antibiotics. *Experientia* **1970**, *26*, 122–123; (c) Waring, M. J.; Wakelin, L. P. G. Echinomycin: a bifunctional intercalating antibiotic. *Nature* **1974**, *252*, 653–657.

21. (a) Jolad, S. D.; Hoffman, J. J.; Torrance, S. J.; Wiedhopf, R. M.; Cole, J. R.; Arora, S. K.; Bates, R. B.; Gargiulo, R. L.; Kriek, G. R. Bouvardin and deoxybouvardin, antitumor cyclic hexapeptides from Bouvardia ternifolia (Rubiaceae). *J. Am. Chem. Soc.* **1977**, *99*, 8040–8044; (b) Pettit, G. R.; Kamano, Y.; Herald, C. L.; Tuinman, A. A.; Boettner, F. E.; Kizu, H.; Schmidt, J. M.; Baczynskyj, L.; Tomer, K. B.; Bontems, R. J. The isolation and structure of a remarkable marine animal antineoplastic constituent: dolastatin 10. *J. Am. Chem. Soc.* **1987**, *109*, 6883–6885.

22. Rüegger, A.; Kuhn, M.; Lichti, H.; Loosli, H.-R.; Huguenin, R.; Quiquerez, C.; Wartburg, A. V. Cyclosporin A, a peptide metabolite from Trichoderma polysporum (Link ex Pers.) Rifai, with a remarkable immunosuppressive activity. *Helv. Chim. Acta* **1976**, *59*, 1075–1092.

23. (a) Kenakin, T. Functional selectivity and biased receptor signaling. *J. Pharmacol. Exp. Ther.* **2010**, *336*, 296–302; (b) Tan, L.; Yan, W.; Mccorvy, J. D.; Cheng, J. Biased ligands of G protein-coupled receptors (GPCRs): structure-functional selectivity relationships (SFSRs) and therapeutic potential. *J. Med. Chem.* **2018**, *61*, 9841–9878.

24. Chatenet, D.; Nguyen, T.-T. M.; Létourneau, M.; Fournier, A. Update on the urotensinergic system: new trends in receptor localization, activation, and drug design. *Front. Endocrinol.* **2013**, *3*, 174.

25. Vaudry, H.; Leprince, J.; Chatenet, D.; Fournier, A.; Lambert, D. G.; Mevel, J.-C. L.; Ohlstein, E. H.; Schwertani, A.; Tostivint, H.; Vaudry, D. International union of basic and clinical pharmacology. XCII. Urotensin II, Urotensin II-related peptide, and their receptor: from structure to function. *Pharmacol. Rev.* **2014**, *67*, 214–258.

26. Federico, A.; Zappavigna, S.; Dallio, M.; Misso, G.; Merlino, F.; Loguercio, C.; Novellino, E.; Grieco, P.; Caraglia, M. Urotensin-II receptor: a double identity receptor involved in vasoconstriction and in the development of digestive tract cancers and other tumors. *Curr. Cancer Drug Targets* **2017**, *17*, 109–121.

27. Clozel, M.; Binkert, C.; Birker-Robaczewska, M.; Boukhadra, C.; Ding, S. S.; Fischli, W.; Hess, P.; Mathys, B.; Morrison, K.; Müller, C.; Müller, C.; Nayler, O.; Qiu, C.; Rey, M.; Scherz, M. W.; Velker, J.; Weller, T.; Xi, J. F.; Ziltener, P. Pharmacology of the Urotensin-II receptor antagonist Palosuran (ACT-058362; 1-[2-(4-benzyl-4-hydroxy-piperidin-1-yl)-ethyl]-3-(2-methyl-quinolin-4-yl)-urea sulfate salt): first demonstration of a pathophysiological role of the Urotensin system. *J. Pharmacol. Exp. Ther.* **2004**, *311*, 204–212.

28. (a) Behm, D. J.; Aiyar, N. V.; Olzinski, A. R.; Mcatee, J. J.; Hilfiker, M. A.; Dodson, J. W.; Dowdell, S. E.; Wang, G. Z.; Goodman, K. B.; Sehon, C. A.; Harpel, M. R.; Willette, R. N.; Neeb, M. J.; Leach, C. A.; Douglas, S. A. GSK1562590, a slowly dissociating Urotensin-II receptor antagonist, exhibits prolonged pharmacodynamic activity *ex vivo*. *Br. J. Pharmacol.* **2010**, *161*, 207–228; (b) Portnoy, A.; Kumar, S.; Behm, D. J.; Mahar, K. M.; Noble, R. B.; Throup, J. P.; Russ, S. F. Effects of Urotensin II receptor antagonist, GSK1440115, in asthma. *Front. Pharmacol.* **2013**, *4*, 54.

29. (a) Douglas, S. A.; Behm, D. J.; Aiyar, N. V.; Naselsky, D.; Disa, J.; Brooks, D. P.; Ohlstein, E. H.; Gleason, J. G.; Sarau, H. M.; Foley, J. J.; Buckley, P. T.; Schmidt, D. B.; Wixted, W. E.; Widdowson, K.; Riley, G.; Jin, J.; Gallagher, T. F.; Schmidt, S. J.; Ridgers, L.; Christmann, L. T.; Keenan, R. M.; Knight, S. D.; Dhanak, D. Nonpeptidic urotensin-II receptor antagonists I: *in vitro* pharmacological characterization of SB-706375. *Br. J. Pharmacol.* **2005**, *145*, 620–635; (b) You, Z.; Genest, J.; Barrette, P. O.; Hafiane, A.; Behm, D. J.; Dorleans-Juste, P.; Schwertani, A. G. Genetic and pharmacological manipulation of Urotensin II ameliorate the metabolic and atherosclerosis sequalae in mice. *Arterioscler. Thromb. Vasc. Biol.* **2012**, *32*, 1809–1816.

30. Liu, D.-G.; Wang, J; Zhang, Z.-T.; Wang, Y. The urotension II antagonist SB-710411 arrests fibrosis in CCL_4 cirrhotic rats. *Mol. Med. Rep.* **2009**, *2*, 953–961.

31. Lee, J. H.; Park, B. K.; Oh, K.-S.; Yi, K. Y.; Lim, C. J.; Seo, H. W.; Lee, B. H. A urotensin II receptor antagonist, KR36676, decreases vascular remodeling and inflammation in experimental pulmonary hypertension. *Int. Immunopharmacol.* **2016**, *40*, 196–202.

32. Kinney, W. A.; Almond, J. H. R.; Qi, J.; Smith, C. E.; Santulli, R. J.; Garavilla, L. D.; Andrade-Gordon, P.; Cho, D. S.; Everson, A. M.; Feinstein, M. A.; Leung, P. A.; Maryanoff, B. E. Structure-function analysis of urotensin II and its use in the construction of a ligand-receptor working model. *Angew. Chem. Int. Edit.* **2002**, *41*, 2940–2944.

33. Brkovic, A; Hattenberger, A.; Kostenis, E.; Klabunde, T.; Flohr, S.; Kurz, M.; Bourgault, S.; Fournier, A. Functional and binding characterizations of Urotensin II-related peptides in human and rat Urotensin II-receptor assay. *J. Pharmacol. Exp. Ther.* **2003**, *306*, 1200–1209.

34. Leprince, J.; Chatenet, D.; Dubessy, C.; Fournier, A.; Pfeiffer, B.; Scalbert, E.; Renard, P.; Pacaud, P.; Oulyadi, H.; Ségalas-Milazzo, I.; Guilhaudis, L.; Davoust, D.; Tonon, M.-C.; Vaudry, H. Structure-activity relationships of Urotensin II and URP. *Peptides* **2008**, *29*, 658–673.

35. Brancaccio, D.; Merlino, F.; Limatola, A.; Yousif, A. M.; Gomez-Monterrey, I.; Campiglia, P.; Novellino, E.; Grieco, P.; Carotenuto, A. An investigation into the origin of the biased agonism associated with the urotensin II receptor activation. *J. Pept. Sci.* **2015**, *21*, 392–399.

36. Billard, É.; Iddir, M.; Nassour, H.; Lee-Gosselin, L.; Molliens, M. P. D.; Chatenet, D. New directions for Urotensin II receptor ligands. *Peptide Science* **2018**, e24056.

37. Castel, H.; Desrues, L.; Joubert, J.-E.; Tonon, M.-C.; Prézeau, L.; Chabbert, M.; Morin, F.; Gandolfo, P. The G protein-coupled receptor UT of the neuropeptide urotensin II displays structural and functional chemokine features. *Front. Endocrinol.* **2017**, *8*, 76.

38. Behrendt, R.; White, P.; Offer, J. Advances in Fmoc solid-phase peptide synthesis. *J. Pept. Sci.* **2016**, *22*, 4–27.

39. Merlino, F.; Yousif, A. M.; Billard, É.; Dufour-Gallant, J.; Turcotte, S.; Grieco, P.; Chatenet, D.; Lubell, W. D. Urotensin II$^{(4–11)}$ azasulfuryl peptides: synthesis and biological activity. *J. Med. Chem.* **2016**, *59*, 4740–4752.

40. Biron, E.; Kessler, H. Convenient synthesis of *N*-methylamino acids compatible with Fmoc solid-phase peptide synthesis. *J. Org. Chem.* **2005**, *70*, 5183–5189.

41. Biron, E.; Chatterjee, J.; Kessler, H. Optimized selective *N*-methylation of peptides on solid support. *J. Pept. Sci.* **2006**, *12*, 213–219.

42. Miller, S. C.; Scanlan, T. S. Site-selective N-methylation of peptides on solid support. *J. Am. Chem. Soc.* **1997**, *119*, 2301–2302.

43. Mitsunobu, O. The use of diethyl azodicarboxylate and triphenylphosphine in synthesis and transformation of natural products. *Synthesis* **1981**, *1*, 1–28.

44. Wisniewski, K.; Koldziejczyk, A. S.; Falkiewicz, B. Applications of the Mitsunobu reaction in peptide chemistry. *J. Pept. Sci.* **1998**, *4*, 1–14.

45. Al-Warhi, T. I.; Al-Hazimi, H. M.; El-Faham, A. Recent development in peptide coupling reagents. *J. Saudi Chem. Soc.* **2012**, *16*, 97–116.

46. Carotenuto, A.; Grieco, P.; Campiglia, P.; Novellino, E.; Rovero, P. Unraveling the active conformation of Urotensin II. *J. Med. Chem.* **2004**, *47*, 1652–1661.

47. Chatenet, D.; Folch, B.; Feytens, D.; Létourneau, M.; Tourwé, D.; Doucet, N.; Fournier, A. Development and pharmacological characterization of conformationally constrained urotensin II-related peptide agonists. *J. Med. Chem.* **2013**, *56*, 9612–9622.

48. Chatenet, D.; Dubessy, C.; Leprince, J.; Boularan, C.; Carlier, L.; Ségalas-Milazzo, I.; Guilhaudis, L.; Oulyadi, H.; Davoust, D.; Scalbert, E.; Pfeiffer, B.; Renard, P.; Tonon, M.-C.; Lihrmann, I.; Pacaud, P.; Vaudry, H. Structure-activity relationships and structural conformation of a novel urotensin II-related peptide. *Peptides* **2004**, *25*, 1819–1830.

49. Batuwangala, M.; Camarda, V.; Mcdonald, J.; Marzola, E.; Lambert, D. G.; Ng, L. L.; Calò, G.; Regoli, D.; Trapella, C.; Guerrini, R.; Salvadori, S. Structure–activity relationship study on Tyr^9 of urotensin-II(4–11): identification of a partial agonist of the UT receptor. *Peptides* **2009**, *30*, 1130–1136.

50. Billard, É.; Létourneau, M.; Hébert, T. E.; Chatenet, D. Insight into the role of urotensin II-related peptide tyrosine residue in UT activation. *Biochem. Pharmacol.* **2017**, *144*, 100–107.

51. Carotenuto, A.; Auriemma, L.; Merlino, F.; Limatola, A.; Campiglia, P.; Gomez-Monterrey, I.; Bianca, R. D. D. V.; Brancaccio, D.; Santicioli, P.; Meini, S.; Maggi, C. A.; Novellino, E.; Grieco, P. New insight into the binding mode of peptides at urotensin-II receptor by Trp-constrained analogues of P5U and urantide. *J. Pept. Sci.* **2013**, *19*, 293–300.

52. Carotenuto, A.; Auriemma, L.; Merlino, F.; Yousif, A. M.; Marasco, D.; Limatola, A.; Campiglia, P.; Gomez-Monterrey, I.; Santicioli, P.; Meini, S.; Maggi, C. A.; Novellino, E.; Grieco, P. Lead optimization of P5U and Urantide: discovery of novel potent ligands at the Urotensin-II receptor. *J. Med. Chem.* **2014**, *57*, 5965–5974.

53. Chatenet, D.; Dubessy, C.; Boularan, C.; Scalbert, E.; Pfeiffer, B.; Renard, P.; Lihrmann, I.; Pacaud, P.; Tonon, M.-C.; Vaudry, H.; Leprince, J. Structure-activity relationships of a novel series of Urotensin II analogues: identification of a Urotensin II antagonist. *J. Med. Chem.* **2006**, *49*, 7234–7238.

54. Billard, E.; Hébert, T. E.; Chatenet, D. Discovery of new allosteric modulators of the urotensinergic system through substitution of the Urotensin II-related peptide (URP) phenylalanine residue. *J. Med. Chem.* **2018**, *61*, 8707–8716.

55. Kim, S.-K.; Li, Y.; Park, C.; Abrol, R.; Goddard, W. A. Prediction of the three-dimensional structure for the rat Urotensin II receptor, and comparison of the antagonist binding sites and binding selectivity between human and rat receptors from atomistic simulations. *ChemMedChem* **2010**, *5*, 1594–1608.

56. Chatenet, D.; Létourneau, M.; Nguyen, Q.; Doan, N.; Dupuis, J.; Fournier, A. Discovery of new antagonists aimed at discriminating UII and URP-mediated biological activities: insight into UII and URP receptor activation. *Br. J. Pharmacol.* **2013**, *168*, 807–821.

57. Chatenet, D.; Nguyen, Q.-T.; Létourneau, M.; Dupuis, J.; Fournier, A. Urocontrin, a novel UT receptor ligand with a unique pharmacological profile. *Biochem. Pharmacol.* **2012**, *83*, 608–615.

58. Ziltener, P.; Mueller, C.; Haenig, B.; Scherz, M. W.; Nayler, O. Urotensin II mediates Erk1/2 phosphorylation and proliferation in GPR14-transfected cell lines. *J. Recept. Signal Transduct.* **2002**, *22*, 155–168.

59. Sauzeau, V.; Mellionnec, E. L.; Bertoglio, J.; Scalbert, E.; Pacaud, P.; Loirand, G. Human Urotensin II-induced contraction and arterial smooth muscle cell proliferation are mediated by RhoA and Rho-Kinase. *Circ. Res.* **2001**, *88*, 1102–1104.

60. Grieco, P.; Carotenuto, A.; Campiglia, P.; Marinelli, L.; Lama, T.; Patacchini, R.; Santicioli, P.; Maggi, C. A.; Rovero, P.; Novellino, E. Urotensin-II receptor ligands. From agonist to antagonist activity. *J. Med. Chem.* **2005**, *48*, 7290–7297.

61. Merlino, F.; Brancaccio, D.; Yousif, A. M.; Piras, L.; Campiglia, P.; Gomez-Monterrey, I.; Santicioli, P.; Meini, S.; Maggi, C. A.; Novellino, E.; Carotenuto, A.; Grieco, P. Structure-activity study of the peptides P5U and Urantide by the development of analogues containing uncoded amino acids at position 9. *ChemMedChem* **2016**, *11*, 1856–1864.

62. Wishart, D. S.; Sykes, B. D.; Richards, F. M. The chemical shift index: a fast and simple method for the assignment of protein secondary structure through NMR spectroscopy. *Biochemistry* **1992**, *31*, 1647–1651.

63. Brancaccio, D.; Limatola, A.; Campiglia, P.; Gomez-Monterrey, I.; Novellino, E.; Grieco, P.; Carotenuto, A. Urantide conformation and interaction with the Urotensin-II receptor. *Arch. Pharm.* **2013**, *347*, 185–192.

64. Chatterjee, J.; Laufer, B.; Beck, J. G.; Helyes, Z.; Pintér, E.; Szolcsányi, J.; Horvath, A.; Mandl, J.; Reubi, J. C.; Kéri, G.; Kessler, H. *N*-Methylated sst_2 selective somatostatin cyclic peptide analogue as a potent candidate for treating neurogenic inflammation. *ACS Med. Chem. Lett.* **2011**, *2*, 509–514.

65. Butini, S.; Gabellieri, E.; Brindisi, M.; Giovani, S.; Maramai, S.; Kshirsagar, G.; Guarino, E.; Brogi, S.; Pietra, V. L.; Giustiniano, M.; Marinelli, L.; Novellino, E.; Campiani, G.; Cappelli, A.; Gemma, S. A stereoselective approach to peptidomimetic BACE1 inhibitors. *Eur. J. Med. Chem.* **2013**, *70*, 233–247.

66. Gaggini, F.; Porcheddu, A.; Reginato, G.; Rodriquez, M.; Taddei, M. Colorimetric tools for solid-phase organic synthesis. *J. Comb. Chem.* **2004**, *6*, 805–810.

67. Breton, B.; Sauvageau, É.; Zhou, J.; Bonin, H.; Gouill, C. L.; Bouvier, M. Multiplexing of multicolor bioluminescence resonance energy transfer. *Biophys. J.* **2010**, *99*, 4037–4046.

68. Hwang, T. L.; Shaka, A. J. Water suppression that works. Excitation sculpting using arbitrary wave-forms and pulsed-field gradients. *J. Magn. Res.* **1995**, *112*, 275–279.

69. (a) Piantini, U.; Sorensen, O. W.; Ernst, R. R. Multiple quantum filters for elucidating NMR coupling network. *J. Am. Chem. Soc.* **1982**, *104*, 6800–6801; (b) Marion. D.; Wüthrich, K. Application of phase sensitive two-dimensional correlated spectroscopy (COSY) for measurements of 1H-1H spin-spin coupling constants in proteins. *Biochem. Biophys. Res. Commun.* **1983**, *113*, 967–974.

70. Braunschweiler, L.; Ernst, R. R. Coherence transfer by isotropic mixing: application to proton correlation spectroscopy. *J. Magn. Reson.* **1983**, *53*, 521–528.

71. Jenner, J.; Meyer, B. H.; Bachman, P.; Ernst, R. R. Investigation of exchange processes by two-dimensional NMR spectroscopy. *J. Chem. Phys.* **1979**, *71*, 4546–4553.

72. States, D. J.; Haberkorn, R. A.; Ruben, D. J. A Two-dimensional nuclear Overhauser experiment with pure absorption phase in four quadrants. *J. Magn. Reson.* **1982**, *48*, 286–292.

73. Bartels, C.; Xia, T.; Billeter, M.; Guentert, P.; Wüthrich, K. The program XEASY for computer-supported NMR spectral analysis of biological macromolecules. *J. Biomol. NMR* **1995**, *6*, 1–10.

74. Wüthrich, K. In NMR of Proteins and Nucleic Acids; John Wiley & Sons: New York, **1986**.

75. Güntert P.; Mumenthaler C.; Wüthrich, K.; Torsion angle dynamics for NMR structure calculation with the new program DYANA. *J. Mol. Biol.* **1997**, *273*, 283–298.

76. Maple, J.; Dinur, U.; Hagler, A. T. Derivation of force fields for molecular mechanics and dynamics from ab initio energy surface. *Proc. Natl. Acad. Sci.* USA **1988**, *85*, 5350–5354.

Table of Contents Graphic (TOC)